https://doi.org/10.5194/egusphere-2024-2079
Preprint. Discussion started: 26 July 2024

Concurrent modes of climate variability linked to spatially compounding wind and precipitation extremes in the Northern Hemisphere

Bastien François[1,*], Khalil Teber[2,*], Lou Brett[3], Richard Leeding[4], Luis Gimeno-Sotelo[5], Daniela I. V. Domeisen[6, 7], Laura Suarez-Gutierrez[7, 8], and Emanuele Bevacqua[9]

[1]Royal Netherlands Meteorological Institute (KNMI), Research and Development Weather and Climate (RDWK), De Bilt, The Netherlands
[2]RSC4Earth, IEF, Leipzig University
[3]Department of Civil and Environmental Engineering, University of Strathclyde, Glasgow, UK
[4]Department of Earth Sciences, Uppsala University, Uppsala, Sweden
[5]Centro de Investigación Mariña, Universidade de Vigo, Environmental Physics Laboratory (EPhysLab), Ourense, Spain
[6]Université de Lausanne, Lausanne, Switzerland
[7]Institute for Atmospheric and Climate Science, ETH Zurich, Zurich, Switzerland
[8]Institut Pierre-Simon Laplace, CNRS, Paris, 75252, France
[9]Department of Compound Environmental Risks, Helmholtz Centre for Environmental Research – UFZ, Leipzig, Germany
[*]These authors contributed equally to this work.

Correspondence: Bastien François (bastien.francois@knmi.nl) and Emanuele Bevacqua (emanuele.bevacqua@ufz.de)

Abstract. Compound wind and precipitation (CWP) extremes often cause severe impacts on human society and ecosystems, such as damage to agricultural crops and infrastructure. High regional frequencies of CWP extremes across multiple regions in the same winter, referred to as spatially compounding events, can further impact the global economy and the reinsurance industry. By combining reanalysis data and climate model simulations, we investigate the influence of two oceanic and two atmospheric variability modes – El Niño Southern Oscillation (ENSO), the Atlantic Multidecadal Variability, the North Atlantic Oscillation (NAO) and the Pacific North American (PNA) – on the frequency of wintertime CWP extremes and associated spatial co-occurrences across the Northern Hemisphere. In many hotspot regions, concurrent variability mode anomalies significantly amplify CWP extreme event frequencies compared to single variability modes. By examining the relationships between CWP extremes across regions, we identify dependencies enabling extreme spatially compounding events with many regions experiencing CWP extremes in the same winter. While ENSO is the most influential variability mode for such extreme spatially compounding events, combinations of modes are essential for the occurrence of these events across the Northern Hemisphere. In particular, combinations of modes amplify both the number of regions and population exposed to CWP extremes in the same winter, for example, they nearly double the number of affected regions compared to neutral conditions on average. Our analysis highlights the importance of considering the interplay between variability modes to improve risk management and mitigation of spatially compounding CWP extremes.

https://doi.org/10.5194/egusphere-2024-2079
Preprint. Discussion started: 26 July 2024

1 Introduction

Weather and climate extremes pose severe risks to human health, infrastructure, natural resources, and ecosystem health. The Intergovernmental Panel on Climate Change (IPCC) Special Report on Managing the Risks of Extreme Events and Disasters to Advance Climate Change Adaptation (SREX) highlighted the importance of exploring compound weather and climate events, defined as the combination of multiple drivers and/or hazards that contribute to societal or environmental risk and have the potential to cause more severe impacts than the respective single hazards (Zscheischler et al., 2018), for improved modelling and risk estimation of extreme weather impacts (IPCC, 2021). Without considering compound extreme weather events, damages from extreme weather events may be either under- or over-estimated (van den Hurk et al., 2023; Hillier et al., 2020). For example, co-occurring compound wind and precipitation (CWP) extremes, the focus of this study, can cause more damage to buildings than high winds or precipitation in isolation because the high winds combined with rainwater can result in severe damage due to the inflow of water through joints or cracks in building structures (Jeong et al., 2020). Going forward, these CWP extremes are likely to change in frequency and/or intensity due to human-induced climate change (IPCC, 2021).

CWP extremes can lead to a range of other exacerbated impacts, such as increased soil erosion (Foulds and Warburton, 2007), agricultural and forestry losses (Van Stan et al., 2011; Ridder et al., 2022), damage to energy infrastructure and buildings (Mirrahimi et al., 2015; Jeong et al., 2020), economic impacts through insurance and disaster recovery (van den Hurk et al., 2023; Ciullo et al., 2023), and human fatalities (Pilorz et al., 2023). Alongside co-occurring extremes in the same location, which correspond to *multivariate events* (Zscheischler et al., 2020), another type of compound event involves the simultaneous occurrence of extremes across multiple regions or locations, referred to as *spatially compounding* extremes (Zscheischler et al., 2020). Spatially compounding events are gaining prominence due to the potential for widespread impacts to affect the global food system, disaster management resources, and (re)insurance industries via large population and asset exposure (Singh et al., 2021; Ciullo et al., 2023; Gampe et al., 2024). For example, widespread spatially compounding flooding throughout nine European countries in June 2013 led to high pressures on trans-national risk reduction and risk transfer mechanisms and €12 billion in losses (Jongman et al., 2014). In the context of simultaneous CWP extremes across multiple regions worldwide, global catastrophe risk pooling could help with reducing the severity of economic shocks (Ciullo et al., 2023). It is thus crucial, in particular for risk management, to better understand CWP extremes and their drivers, including the spatial dependencies between the different regions that can amplify spatially compounding risks.

Multiple drivers can lead to CWP extremes, with their influence varying across different geographical regions (Dowdy and Catto, 2017). The ultimate drivers of CWP extremes are typically atmospheric rivers (Waliser and Guan, 2017), low-pressure systems (e.g., Seneviratne et al., 2012; Wahl et al., 2015) including tropical (Zhang et al., 2021) and extratropical (Manning et al., 2024) cyclones, fronts (Raveh-Rubin and Catto, 2019), convective storms (Dowdy and Catto, 2017). Accordingly, regions prone to cyclones are particularly exposed to CWP extremes (Martius et al., 2016; Messmer and Simmonds, 2021; Owen et al., 2021). At the global scale, such drivers are modulated by modes of atmospheric and oceanic variability, which represent variations in atmospheric patterns due to internal climate variability. For example, the Pacific North American (PNA) pattern and the North Atlantic Oscillation (NAO) are two dominant modes of interannual midlatitude climate variability during the

https://doi.org/10.5194/egusphere-2024-2079
Preprint. Discussion started: 26 July 2024

Northern Hemisphere winter. During extreme phases of the PNA and NAO, the intensity and location of storms and moisture transport deviate from mean conditions over the Pacific-North American region (Wallace and Gutzler, 1981a; Xie et al., 2020) and the Euro-Atlantic region (Hurrell et al., 2003; Lodise et al., 2022), respectively. Oceanic modes of variability such as the El Niño Southern Oscillation (ENSO) and the Atlantic Multidecadal Variability (AMV) can further modulate atmospheric modes of variability and compound extremes. ENSO, for example, can influence both the PNA and NAO (Jiménez-Esteve and Domeisen, 2019, 2020; Müller and Roeckner, 2006) as well as weather systems in many regions worldwide (Zhao, 2015; van Oldenborgh et al., 2005; Domeisen et al., 2019). The AMV, an alteration of warm and cold sea surface temperatures in the North Atlantic on decadal timescales, has been shown to influence the intensity and frequency of Atlantic hurricanes (Trenberth and Shea, 2006; Wang et al., 2022) and the long-term variability of the NAO (Davini et al., 2015). Due to the complex teleconnections linking these four climate modes (ENSO, NAO, PNA, and AMV) (e.g., Müller and Roeckner, 2006; Pinto et al., 2009; O'Reilly et al., 2024; Trascasa-Castro et al., 2021; Davini et al., 2015) and their influence on weather patterns across the Northern Hemisphere, in this study we select these modes as potential modulators of wintertime CWP extremes across the Northern Hemisphere. Note that among the selected modes, some are themselves specific phenomena that are internally driven, such as ENSO, while others are a representation of the dominant weather and climate variability in a particular region, such as the NAO or the PNA.

We investigate the effects of these modes of variability and their combinations on wintertime CWP extremes across the Northern Hemisphere using reanalyses and large ensemble climate model simulations from the CESM General Circulation Model (Kay et al., 2015). Specifically, we (1) analyse the influence of modes of variability on wintertime regional frequencies of CWP extremes in individual regions across the Northern Hemisphere. Furthermore, we investigate spatially compounding events with many regions (or large numbers of people) under high CWP extreme frequencies in the same winter by examining the effect of (2) dependencies between CWP extremes across different regions and (3) combinations of modes of variability on such spatially compounding events. Finally, we (4) inspect the atmospheric circulation anomalies associated with the considered compound events. We focus on the Northern Hemisphere due to the high population density and the severe impacts of CWP extremes in this part of the world (e.g., Liberato, 2014; Wahl et al., 2015; Raveh-Rubin and Wernli, 2015). The winter season is considered as most storms and CWP extremes occur over this season across the Northern Hemisphere (Greeves et al., 2007; Hansen et al., 2019), and modes such as NAO and ENSO are most effective during winter (Krichak and Alpert, 2005; Toniazzo and Scaife, 2006). Using large ensemble climate model simulations provides a large sample size that enables a robust model-based analysis of the effects of rare concurrent variability mode anomalies on low probability CWP extremes (van der Wiel et al., 2019; Singh et al., 2021; Raymond et al., 2022; Bevacqua et al., 2023; Qian et al., 2023; Wang et al., 2023).

The study is structured as follows: Sect. 2 describes the data used, as well as the methodology to analyse the effects of variability modes on CWP extremes and spatially compounding events. Results are provided in Sect. 3. Conclusions, discussions, and perspectives for future research are presented in Sect. 4.

https://doi.org/10.5194/egusphere-2024-2079
Preprint. Discussion started: 26 July 2024

2 Data and Methods

We examine the influence of four variability modes on CWP extremes across 25 selected regions in the Northern Hemisphere defined in the SREX (Iturbide et al., 2020, see Fig. 1).

2.1 Model and reanalysis data

We employ model simulations from the coupled Community Earth System Model (CESM; spatial resolution of 1.25° by 1.25°), which provides forty ensemble members (Kay et al., 2015). These ensemble members are derived from the CESM model under the same model physics and external forcings, with each of the members starting in 1920 and initialised via slightly different initial states, leading to different evolutions from internal climate variability (Maher et al., 2021). Considering multiple members provides a large sample size that allows for assessing the effect of internal climate variability and infrequent combinations of modes of variability on rare compound events (Bevacqua et al., 2023; Singh et al., 2021). For daily wind and precipitation data, the historical period simulations (1950–2005) are extracted and extended until 2019 using the emission scenario associated with a radiative forcing of $+8.5\text{W.m}^{-2}$ (RCP 8.5 scenario), resulting in a total of $70 \times 40 = 2800$ years of data.

To evaluate the CESM model, we employ ERA5 reanalysis data (Hersbach et al., 2020) (spatial resolution of 0.25°) for the period 1959-2019 (Singh et al., 2021), from which we derive daily means of wind speed and precipitation via averaging sub-daily data.

Seasonal indices for the two oceanic (ENSO and AMV) and two atmospheric (NAO and PNA) variability modes for both CESM and ERA5 data are calculated from monthly data using the National Center for Atmospheric Research (NCAR) data package Climate Variability Diagnostics Package (CVDP, Phillips et al., 2014). The indices for the NAO, PNA and AMV are computed for the December–February periods, while for ENSO we extract November–January to account for lagged effects (Li et al., 2011; Hong Lee et al., 2023). For each mode, we defined their positive and negative phases when the index is above or below its mean by $+1$ standard deviation, respectively, otherwise the phase is considered neutral.

2.2 Methods

2.2.1 CWP extremes

To investigate winter season (December–February) CWP extremes at the grid cell level we derived seasonal counts of CWP extremes, defined as wind and precipitation values simultaneously exceeding high thresholds. This results in one count per season per grid cell, which allows for investigating the effect of seasonally-averaged climate variability modes on the counts. We use the 98th percentile of wind and precipitation over the 1950–2019 period for the main analysis based on data from the CESM model. For model evaluation, we use the 95th percentiles over the 1950-2019 period – such a lower threshold allows for a more robust evaluation, given the ERA5's limited period (Bevacqua et al., 2021b; Kelder et al., 2022; Fischer et al., 2023).

https://doi.org/10.5194/egusphere-2024-2079
Preprint. Discussion started: 26 July 2024

2.2.2 Regional and spatially compounding effects of combined variability modes

To investigate the effect of variability modes on CWP extremes, we use three different metrics. The first metric allows for assessing the effect of modes in individual regions:

- **(Metric 1)** Regionally averaged counts of CWP extremes. CWP counts are averaged by region over landmasses, weighted by the cosine of latitude. This metric allows us to assess the effects of variability modes on individual regions separately.

As Metric 1 is derived for each region individually, the influence of variability modes on the high regional frequencies of CWP extremes across multiple regions in the same winter (i.e., spatially compounding events) cannot be deduced. Therefore, we introduce two additional metrics to investigate the effects of variability modes on high frequencies of regional CWP extremes across multiple regions in the same winter (Metric 2) and on the total population of the Northern Hemisphere exposed to CWP extremes in the same winter (Metric 3).

- **(Metric 2)** Total number of affected regions during the same winter. For a given winter, a region is considered as affected by CWP extremes when the regionally averaged count of CWP extremes (Metric 1) is above its 80th percentile derived from the distribution of the 1950-2019 period. Then, the total number of affected regions during the same winter is counted.

- **(Metric 3)** Total population exposure. To assess the effects of variability modes on the population of the Northern Hemisphere exposed to CWP extremes during the same winter, we calculated for each winter the weighted averages of CWP extremes $wCWP$ (hereafter referred to as "population-weighted CWP extremes") using CWP extremes and population counts at the grid cell level as follows:

$$wCWP = \frac{\sum_{i=1}^{N_{grid}} N_{CWP_i} \times Pop_i}{\sum_{i=1}^{N_{grid}} Pop_i}$$

where N_{CWP_i} and Pop_i are the seasonal counts of CWP events and the population count at grid cell i, respectively, and N_{grid} is the total number of grid cells over the Northern Hemisphere. For this purpose, global population counts for the year 2020 from the GPW product have been used (Columbia University, 2016).

2.2.3 Identifying relevant effects of single and combined variability modes for the regional and spatial metrics

We quantify the effect of a positive (or negative) phase of a single variability mode of interest on CWP extremes based on the ratio between (i) CWP metrics under the positive (or negative) phase of the mode of interest, while additionally conditioning the other modes in a neutral state, and (ii) CWP metrics under all variability modes in neutral phase. Hereafter, we referred to this effect as *direct effect*. Following Singh et al. (2021), additionally conditioning all other modes in the neutral phase in (i) allows for better isolating the causal effects of the individual variability mode of interest. Despite such additional conditioning, some confounding effects may remain, particularly because modes in neutral states still vary within the range of neutral conditions

https://doi.org/10.5194/egusphere-2024-2079
Preprint. Discussion started: 26 July 2024

and we do not control for them, and further effects may arise from variability mode not considered in this study. Similarly to the analysis of single variability modes, we quantify the effect of concurrent variability modes in non-neutral phases based on the ratio between (i) CWP metrics under the concurrent modes of interest while conditioning all other modes to neutral conditions and (ii) CWP metrics under all variability modes in neutral phase. In terms of notation, we refer to concurrent climate variability modes by specifying (positive and negative) phases of NAO, PNA, ENSO and AMV in this order, with unspecified modes being in neutral states.

Although the main part of our study is based on the analysis of the metrics defined in subsection 2.2.2, we provide an overview of the direct (resp. combined) effects of modes on CWP extreme frequencies at the grid cell level in Fig. 2 (resp. Fig. 7). Results for the effects of variability modes on regionally averaged metric (Metric 1) and spatial metrics (Metrics 2 and 3) ratios are presented in Figs. 3, 4, and 6. For both regional and spatially compounding cases, we focus on the modes of variability influences leading to an increase in the means of the different metrics compared to neutral conditions (hereafter referred to as *positive effects*). That is, in this study, we do not investigate the influence of variability modes on the decrease of the metrics. When results for the different metrics are presented with box plots (Figs. 3, 5 and 6), interquartile range and mean of the distribution are displayed.

Given the focus on four variability modes, each with three possible phases, there are, in principle, eighty-one possible phase combinations, motivating the need for a synthesis of their effects. When presenting the results in Sect. 3, we focus our analysis on individual and concurrent variability modes having a *significant and positive* effect on the different metrics using permutation tests (see subsection 2.2.4). To support the interpretation of the effects of concurrent variability modes on CWP metrics, in Figs. 3 and 6 we also show the effects of all univariate variability modes that contribute to the concurrent modes with significant effects regardless of whether they exert a significant effect in isolation compared to neutral conditions or not. Furthermore, to ensure robustness in the results, we disregard concurrent variability modes that occur very rarely by only considering concurrent variability modes with an empirical return period, defined as the inverse of their relative frequency, greater than 280 years (i.e., occurring for more than 10 years in our 2800 years dataset). It should be noted here that the empirical return periods for concurrent modes provided in this study are conditional as they are calculated by conditioning all other modes to neutral conditions. To provide an overview of the synthesis of the variability modes, effects of all possible concurrent modes are displayed for regionally averaged metric in Figs. S8-S14 (for a selection of regions for the sake of brevity) and spatial metrics in Fig. S15.

Finally, to provide insights into possible *amplified effects of concurrent variability modes* (Singh et al., 2021) relative to the effects of the modes that contribute to such combination, we identify combinations for which the average metric is higher than that of the *underlying mode sub-combinations* (note that no test here is performed, so this should be interpreted carefully, see explanations in subsection 2.2.4). For example, the concurrent modes NAO-PNA+ENSO+ are deemed to possibly have an amplified effect relative to the underlying mode sub-combinations if the average metric under NAO-PNA+ENSO+ is higher than the underlying mode sub-combinations, which are NAO-, PNA+ and ENSO+ taken in isolation, as well as the bivariate mode sub-combinations NAO-PNA+, NAO-ENSO+ and PNA+ENSO+. The identified combinations with amplified effects are highlighted in Figs. 3, 4, 6 and 7 via dark blue box plots and boxes.

https://doi.org/10.5194/egusphere-2024-2079
Preprint. Discussion started: 26 July 2024

2.2.4 Permutation test procedure to assess significance in effects of combined variability modes

As already mentioned in subsection 2.2.3), the statistical significance of the effects of individual and concurrent variability modes on CWP metrics compared to neutral conditions is assessed using permutation tests (Good, 2013; DelSole et al., 2017; Singh et al., 2021). Specifically, for a given CWP metric, we test whether the ratio of the average of the metric associated with a given set of phases of interest (e.g., NAO+ENSO-, set as the numerator) to the average of the metric under neutral conditions (set a denominator) is larger than one at significance level $\alpha = 0.10$ based on one-sided tests. To test the hypothesis that the average of the metric under individual and concurrent variability modes is higher than under neutral conditions, we compared the ratio obtained from the original samples with a confidence interval of the ratio obtained from data without an effect of the modes on the CWP metric. Specifically, the latter was obtained via randomly permuting without replacement the samples for both numerator and denominator, and re-estimate the ratio from the resampled data. By repeating this procedure several times, we can then define a confidence interval for the ratio and a critical region for test rejection. If the original ratio is higher than the $(1-\alpha)*100$th percentile, the average of the metric associated with the set of phases of interest is considered to be significantly higher than that of the neutral conditions. As several tests are carried out for the different concurrent modes, a Bonferroni correction (Bonferroni, 1936; Sedgwick, 2014) is applied to control the overall probability of Type I (or false positive) errors. Please note that, while identifying concurrent variability modes with significantly *amplified* effects relative to the effects of the modes that contribute to such combination is relevant, it has not been done in this study as no statistically consistent procedure including Bonferroni correction has been found for such a statistical problem. For example, to identify the concurrent modes NAO+ENSO+AMV+ as having a significantly amplified effect on the metrics, six permutation tests comparing the effects of NAO+ENSO+AMV+ against those of its six sub-combinations must all reject the equality of effects. Designing such a statistical test procedure while controlling the false discovery rate goes beyond the scope of the present study and is therefore not included in the analysis. In addition, in Figs. 2 and 7 only, we assess whether averages of the CWP extreme frequencies at the grid cell level associated with a given set of phases are significantly different compared to neutral conditions (i.e., not necessarily larger). For these tests performed at the grid cell level, we use two-sided permutation tests. In this case, the critical region for rejection is defined using the $(\frac{\alpha}{2}) \times 100$th and $(1-\frac{\alpha}{2}) \times 100$th percentiles.

Regarding the number of samples m for permutation tests, several trials showed that choosing $m = 100.000$ allows us to obtain robust results for the three different metrics. Thus, the analysis of the three metrics was carried out using $m = 100.000$. However, when applied to the grid cell level for Figs. 2 and 7, results from permutation tests proved less sensitive to the choice of the number of sample, and m was chosen to be equal to 100.

3 Results

Before investigating the effect of individual variability modes and concurrent modes on CWP extremes and associated spatially compounding events in CESM simulations for the 1950-2019 period, we carried out a model evaluation with respect to ERA5 over the 1959-2019 period. Such a model evaluation is mainly performed for the effects of individual variability modes, as a robust assessment of the effects of concurrent variability modes requires a large sample size (Singh et al., 2021). For the same

https://doi.org/10.5194/egusphere-2024-2079
Preprint. Discussion started: 26 July 2024

reason, the effects of individual variability modes in ERA5 are evaluated without constraining the other modes to be in the neutral phase (which thus differs from the *direct effects* of variability modes defined in subsection 2.2.3).

Results for model evaluation are displayed in Figs. S1-S5 of the Supplement. Although the simulated CWP absolute frequencies exhibit some biases with respect to ERA5 over the Northern Hemisphere (Fig. S1), CESM provides an adequate representation of the anomalies in CWP frequencies induced by individual variability modes relative to neutral conditions (Figs. S2-S5). We conclude from this model evaluation that CESM is suitable for further investigating the CWP extremes and their relationships with variability modes. In the following, we assess the effect of modes of variability and their combinations on CWP extremes via the CESM model based on the 98th percentiles, and also provide a one-to-one comparison with ERA5 based on the same percentiles.

3.1 Direct effects of variability modes on regional CWP extremes

The direct effects of variability modes on CWP extremes in CESM simulations (Fig. 2) are in general agreement with existing literature, showing that differing phases of NAO, PNA and ENSO significantly modulate CWP extreme frequencies over multiple regions of the Northern Hemisphere. Table S1 provides a concise summary of the agreement between CESM simulations and existing literature. Within Europe, NAO+ and NAO- significantly increase CWP extremes in Northern Europe (NEU) and the Mediterranean region (MED) respectively (Figs. 2a and 2b), in agreement with studies such as (Pinto et al., 2009; Hurrell and Deser, 2010). Specifically, the NAO+ regime is associated with stronger than average westerlies in Northern Europe, with Atlantic storm activity being shifted northeastward (Hurrell and Deser, 2010) and favouring CWP extremes. NAO+ also significantly influences CWP extremes in North Asia. An enhancement of CWP extremes over Russian-Arctic (RAR) and Western Siberia (WSB) during NAO+ (Fig. 2a) aligns with low-pressure systems transiting from the North Atlantic toward Northern Europe, which lead to an intensified, northeastward tilted storm track roughly directed toward the Arctic at its exit (Pinto and Raible, 2012). The low pressure associated with storms under NAO+ is accurately represented in CESM simulations (Fig. S6a), with negative pressure anomalies partially or fully covering the regions experiencing a significant increase in CWP extremes. However, an exception is found for Northeastern North America (NEN) during NAO-, where high sea level pressure anomalies of $\sim +3$ hPa are associated with increased CWP extremes. While no regions experience increased CWP extremes under PNA+ (Fig. 2c), PNA- significantly increases CWP extremes compared with neutral conditions in Eastern Siberia (ESB) and Russian Far East (RFE) within North Asia (Fig. 2d), and in Northeastern North America (NEN), Northwestern North America (NWN) and Western North America (WNA) in the North America macroarea. These results likely arise due to increased blocking in the Pacific during PNA- (Li et al., 2017), increasing storm frequency in the northern Pacific.

Among the oceanic modes of variability ENSO and AMV, the former has the most relevant effects. ENSO+ (Fig. 2e) increases CWP extremes across the Arabian Peninsula (ARP), where a substantial fraction of precipitation variability is influenced by equatorial Pacific sea surface temperatures associated with ENSO (Niranjan Kumar and Ouarda, 2014). A possible mechanism for the increased precipitation is that the anomalous warming in the central and eastern Pacific Ocean during ENSO+ alters the mean position of the subtropical jet stream during winter months (Niranjan Kumar and Ouarda, 2014). A significant effect of ENSO+ is also found for the two other regions of Africa (Sahara SAH and Western Africa WAF), although

https://doi.org/10.5194/egusphere-2024-2079
Preprint. Discussion started: 26 July 2024

no related papers have been found in the literature. In addition, ENSO+ exhibits a statistically significant direct effect on East North America (ENA) (Yeh et al., 2018) and North Central America (NCA) (Taschetto et al., 2020), in association with ~ -1.5 hPa sea level pressure anomalies (Fig. S6e). Some significant effects of ENSO+ are also found in Central South Asia, in Eastern Central Asia (ECA) and Western Central Asia (WCA), although no papers report these effects. For ENSO- (Fig. 2f), CWP extremes are significantly increased for two regions within Central-South Asia: South Asia (SAS) and East Asia (EAS). For the AMV, we find no significant regional effects of AMV+ and AMV- conditions (Figs. 2g and 2h), in line with weak sea level pressure anomalies associated with AMV phases, ranging from ~ -1.5 to $\sim +1.5$ hPa (Figs. S6g and S6h).

3.2 Effects of concurrent anomalies in variability modes on regional CWP extremes

Model simulations (CESM) show that not only individual variability modes can have effects on regional wintertime frequencies of CWP extremes, but also combinations of modes (Fig. 3; Fig. S7 shows the same but for absolute frequencies). Figure 4 provides a summary of these effects, including the count of modes combinations (including both individual modes and concurrent modes) that enhance CWP extremes compared to neutral conditions for each region (see numbers on the right side of the matrix in Fig. 4). For example, Northern Europe (NEU) exhibits the highest count of mode combinations that significantly enhance CWP extreme frequencies compared to neutral conditions, with eleven mode combinations that all involve NAO+. Another example is Northern Central America (NCA), the Arabian Peninsula (ARP), and Western Central Asia (WCA), where nine combinations involving ENSO+ significantly enhance CWP extreme frequencies. In the following we move to discussing the effects of relevant mode combinations and regions in more detail.

Model simulations (CESM) show that concurrent anomalies in variability modes amplify the effects of individual modes in many regions. For the Mediterranean region (MED) in Europe (Fig. 3a), five concurrent variability modes containing NAO- have significant positive effects with respect to neutral conditions, in agreement with the relevance of NAO- (Pinto et al., 2009). Among these five concurrent variability modes, three combinations of modes have an amplified effect relative to the underlying mode sub-combinations (blue boxes). For example, in the MED region, CWP extremes are on average ~ 1.5 times more likely under the concurrent mode NAO-ENSO+ than under neutral conditions, while being ~ 1.1 and ~ 1.2 times more likely for NAO- and ENSO+ in isolation. However, the empirical return period of NAO-ENSO+ is 65 years, while it is equal to 20 and 30 years for NAO- and ENSO+, respectively, which means that the concurrent mode NAO-ENSO+ is ~ 3 and ~ 2 times less likely to occur in any given year than NAO- or ENSO+ in isolation. However, it should be noted that the empirical return periods provided here for concurrent modes are conditional, that is they are calculated by conditioning all other modes in the neutral phase. Therefore, despite providing an indication of the rarity of concurrent modes, they should not be considered as absolute return periods as, by construction, they are larger than the unconditional return periods obtained without conditioning the other modes in neutral conditions.

Concurrent modes can also amplify CWP extreme frequencies in other regions. For example, in the Arabian Peninsula (ARP) within Africa, CWP extremes are on average ~ 3.5 times more likely than neutral conditions under ENSO+; however, when ENSO+ combines with NAO-PNA+, CWP extremes are on average ~ 4 times more likely, while both individual modes (NAO- and PNA+) do not have a significant effect on the mean frequency of CWP extreme frequencies relative to neutral conditions.

https://doi.org/10.5194/egusphere-2024-2079
Preprint. Discussion started: 26 July 2024

Furthermore, within the Sahara (SAH), a CWP extreme is on average ~ 2 times more likely to occur under ENSO+AMV- conditions than neutral conditions, while being ~ 1.5 and ~ 0.5 times more likely under ENSO+ and AMV- in isolation. The combination of NAO-ENSO+ has an amplified effect relative to the underlying mode sub-combinations in all three African regions, increasing approximately the likelihood of CWP extremes frequencies by a factor of ~ 4, 1.5 and 2 relative to neutral conditions in the Arabian Peninsula (ARP), Sahara (SAH) and Western Africa (WAF), respectively, with an empirical return period of 65 years. PNA+ENSO+ and ENSO+AMV- also increase the likelihood of CWP extremes in both ARP and SAH, and the combination NAO-PNA+ENSO+ only increases the likelihood of CWP extremes relative to neutral conditions, within the ARP region of Africa.

The Central North America (CNA) region exemplifies how the effects of individual modes can combine to significantly increase CWP extreme frequencies in a given winter relative to neutral conditions, even if individual modes do not exert significant effects in isolation. For example, despite the fact that both PNA+ and ENSO+ in isolation do not significantly increase CWP extremes (indicated by no grey arrows in Fig. 3b), combined PNA+ENSO+ increases significantly the likelihood of CWP extremes by a factor of ~ 1.5 compared to neutral conditions (indicated by the grey arrow and blue box). Furthermore, within North America, the region with the most combinations of modes that present amplified effects on CWP extreme frequencies is East North America (ENA), with six separate combinations (see blue boxes). Of these combinations, ENSO is always in the positive phase and PNA+ENSO+ has the lowest empirical return period of 48 years.

No variability modes within this study influenced the Caribbean (CAR) or South Central America (SCA). However, these regions are relatively small, and it is likely that the coarser-resolution orography in the CESM negatively affects the representation of CWP extremes in these regions (e.g., Iles et al., 2020). Similarly, in the Greenland/Iceland region, no concurrent variability modes showed a significant increase in CWP extremes relative to neutral conditions. CWP extremes in the regions where the different combinations of the variability modes NAO, ENSO, PNA and AMV had no significant effects might be affected by other variability modes (see final Discussion).

Concurrent variability modes increase CWP extreme frequencies relative to neutral conditions in North Asia by ~ 1.5 to ~ 2 times relative to neutral conditions depending on the combination. PNA-ENSO- increases the likelihood of CWP extreme frequencies by ~ 1.5 times in three of North Asia's four regions (Eastern Siberia ESB, Russian-Arctic RAR and Russian Far East RFE), with a return period of 48 years. PNA-AMV- also increases the likelihood of CWP extremes by ~ 1.5 times in RFE, with a return period of 58 years. NAO+PNA- and NAO+ENSO+AMV- increase the likelihood of CWP extremes in Western Siberia (WSB) only by a factor of ~ 1.5 and ~ 2 relative to neutral conditions, respectively. NAO+ENSO+AMV- conditions increases the likelihood of CWP extremes by the largest factor in North Asia, however, the empirical return period is 215 years, thus these conditions are less likely to occur than the other concurrent variability modes (Fig. 3).

Within Central South Asia, the Tibetan-Plateau (TIB) exemplifies again how individual modes without significant effects on CWP extremes (here, AMV- and ENSO+) can combine to significantly increase the likelihood of CWP extremes during winters. Across the five regions of Central South Asia, all concurrent modes that, on average, led to more CWP extremes than their underlying mode sub-combinations (blue boxes) include the variability mode ENSO. Of these concurrent modes, ENSO

https://doi.org/10.5194/egusphere-2024-2079
Preprint. Discussion started: 26 July 2024

is always in the positive phase within the inland regions (ECA, TIB and WCA); while being in the negative phase in the coastal regions (EAS and SAS).

Regarding the comparison of CESM results with those of ERA5, the range of CESM ratios of regionally averaged CWP extreme frequencies with respect to neutral conditions generally covers most of the time the values for ERA5 for the different concurrent modes, when available (Fig. 3).

Results from Fig. 3 and the summary in Fig. 4 cannot be used to conclude whether the effects of concurrent variability modes lead to spatially compounding CWP extremes, that is high wintertime frequencies of CWP extreme across multiple regions during the same winter. These figures illustrate the effect of individual and concurrent variability modes on regionally averaged CWP extreme frequencies, which are derived for each region separately. For example, it shows that ENSO+ significantly modulate regionally averaged CWP extreme frequencies for North America and Central Asia, but – in principle – a possibility could be that half of the winter seasons with ENSO+ leads to a significant increase of CWP extremes for North America only, while the other half affects Central Asia, therefore not simultaneously. Nevertheless, the number of regions where each mode combination has significant effects in Fig. 4 (see numbers on the top of the matrix) suggests that some mode combinations may potentially lead to spatially compounding CWP extremes. For example, NAO-ENSO+ significantly enhances regional CWP extreme frequencies in eight regions, which means that if these regional effects of NAO-ENSO+ can manifest in the same winter, NAO-ENSO+ would lead to spatially compounding CWP extremes. We clarify whether individual and concurrent variability modes can lead to concurrent CWP extremes during the same winters across regions in the next section.

3.3 Effects of concurrent variability modes on spatially compounding CWP extremes

The presence of mode phases that have an effect on CWP extremes in multiple regions suggests the potential for spatially compounding events, that is high frequencies of CWP extremes across multiple regions during the same winter. In general, dependencies between counts of CWP extremes in different regions can favour such spatially compounding events (Bevacqua et al., 2021a) because regions connected by positive dependencies tend to experience CWP extremes at the same time. Thus, as a first step in the investigation of spatially compounding events, we analyse such dependencies. This also provides preliminary information on groups of regions that may be affected by CWP extremes during the same winters. Figure 5a shows Spearman correlations of regionally averaged CWP extreme frequencies (Metric 1) between all pairs of regions. Regions that are geographically close tend to be positively correlated (see correlation values in contoured black boxes), in line with spatial autocorrelation. However, also some regions that are from different macroareas and therefore more distant can be correlated, e.g., Central-South Asian regions with African regions or North American regions with North Asian regions. This highlights the potential for underlying effects of modes of variability that can connect distant regions. Notably, Fig. 5a highlights that most of the pair correlations between CWP extreme counts in different regions are positive.

In line with such dominant positive correlations (Fig. 5a), we find that dependencies among regions overall enhance the potential for spatially compounding events. Specifically, we compare the number of affected regions (Metric 2) from the original dataset with the number obtained after breaking the dependencies via randomly shuffling regional CWP extreme counts using bootstrap in all regions in time (Bevacqua et al., 2021a). As a result, the distribution of the number of regions

https://doi.org/10.5194/egusphere-2024-2079
Preprint. Discussion started: 26 July 2024

affected during the same winters is different from that obtained by assuming independence between regions (Fig. 5b), with dependencies elongating both tails of the distribution. For spatially compounding extremes on the right tail of the distribution, this implies a higher 50-year return level for the number of regions affected by high CWP counts in the same winter compared to independence, that is 11 instead of 9 affected regions (see vertical lines). Consistent with findings in Bevacqua et al. (2021a), this dependency-driven shift is not observed for the mean of the distribution (not shown).

The increased count of regions under CWP extremes due to the dependencies among regions can be linked to modes of variability. That is, the high number of regions simultaneously affected by CWP extremes, which is possible due to the dependencies among regional CWP extremes, would also not be possible without the effects of concurrent variability modes (Fig. 5c). In particular, when all variability modes are neutral, on average around four regions are affected simultaneously by high regionally averaged CWP extremes. Generally, as the number of variability modes in anomalous conditions increases, the likelihood of multiple regions simultaneously experiencing extreme conditions also increases (Fig 5c; see letters indicating significant differences among distributions, with the exception of the distributions related to three and four modes). Notably, this effect is even more marked when focusing on winter seasons with an extreme number of regions affected (right whiskers of the boxplots). Overall, these results indicate that concurrent anomalies in variability modes are key for spatially compounding events.

Given the dependencies among regions and that combinations of variability modes are essential for spatially compounding CWP extremes, we move to identify which are the relevant mode combinations that enhance the number of regions affected by CWP extremes (Metric 2) and population exposed to CWP extremes (Metric 3). We find that thirteen individual and concurrent variability modes significantly increase the number of affected regions compared to neutral conditions (Fig. 6a). Three bivariate combinations have a significant effect on the total number of affected regions and an amplified effect relative to the underlying modes contributing to these combinations (see blue boxes for ENSO+AMV-, PNA+ENSO+ and NAO-ENSO+). NAO-ENSO+ nearly doubles the number of regions simultaneously exposed to CWP extremes on average relative to neutral conditions. Please note that, although not examined here, causal links among climate variability modes and oceanic modes exist, which might be relevant to investigate, including their effects on spatially compounding events (see final Discussion). For example, ENSO+ is present in ten of the thirteen sets of modes with significant effects (see "+" sign in Fig. 6a), highlighting the key role of ENSO+ for spatially compounding events.

In terms of population exposed to CWP extremes, four combinations (ENSO-AMV+, NAO-PNA+ENSO+, NAO+ENSO-AMV+ and PNA-ENSO-) are identified as having a significant effect compared to neutral conditions (Fig. 6b). Among these four combinations, only one (NAO-PNA+ENSO+) has already been identified as having a significant effect on the number of affected regions in Fig. 6a, highlighting that the heterogeneous distribution of population density across regions needs to be considered to assess the societal vulnerability to CWP extremes. In particular, variability modes in isolation do not lead to significant effects on the population exposure compared to neutral conditions, indicating the importance of considering combinations of modes to distil the effects of modes of variability on the population affected. Notably, while ENSO+ dominates the influence of modes of variability on the number of affected regions (see "+" sign in Fig. 6a), ENSO- dominates for the population affected (see "−" sign in Fig. 6b).

https://doi.org/10.5194/egusphere-2024-2079
Preprint. Discussion started: 26 July 2024

3.4 Physical mechanisms underlying spatially compounding CWP extremes

We now move to investigating the physical mechanisms leading to spatial co-occurrences of CWP extremes by analysing SLP anomalies for concurrent variability modes with significant effects on spatially compounding events (Fig. 7). We restrict the analysis to the seven combinations having an amplified effect relative to their underlying mode sub-combinations on Metric 2 and Metric 3 (i.e. combinations with blue boxes in Fig. 6): namely, NAO-ENSO+, PNA+ENSO+ and ENSO+AMV- for affected regions (Fig. 6a) and PNA-ENSO-, ENSO-AMV+, NAO+ENSO-AMV+ and NAO-PNA+ENSO+ for exposed population (Fig. 6b). These combinations have a reasonably low return period (leq82 years), thus are not very unlikely events in the model simulations.

The largest positive effects on the number of affected regions (Fig. 6a) is observed under concurrent ENSO+ (El Niño phase) and NAO-, that is NAO-ENSO+ (Figs. 7a and 7b). Under such a combination of modes of variability NAO-ENSO+, negative SLP anomalies patterns intensify and expand over the North Atlantic Ocean compared to those for modes NAO- and ENSO+ in isolation (Figs. S6b and S6e). This results in significantly more CWP extremes (Metric 1) than under individual effects of NAO- and ENSO+ over many regions of North America, North Central America, Europa and Africa. Among the affected regions under NAO-ENSO+ are West Africa (WAF), the Arabian Peninsula (ARP) and the Sahara (SAH), three very dry regions for which the absolute frequency of extreme CWPs is low (see Fig. S1). Over Europe, the identified wintertime effect of NAO-ENSO+ is in agreement with known effects of NAO-, associated with an equatorward shift of the storm track over the North Atlantic (Rogers, 1997; Rivière and Orlanski, 2007). We note that the occurrence of the NAO-ENSO+ mode combination is favoured by the fact that El Niño conditions (ENSO+ phase) are conducive to NAO- via a range of different pathways, the most dominant of which is through the stratosphere (Domeisen et al., 2015).

ENSO exhibits a strong teleconnection to the North Pacific and the PNA (Wallace and Gutzler, 1981b; Garfinkel and Hartmann, 2008; Hu et al., 2023), leading to ENSO+ and PNA+ to occur at high frequency. Such a PNA+ENSO+ combination (Figs. 7c and 7d) intensifies the negative SLP anomalies patterns on both sides of North America with respect to PNA+ and ENSO+ modes in isolation (Figs. S6c and S6e), mainly amplifying CWP extreme frequencies for regions within North America, Central America and Africa. In contrast, when ENSO+ combines with AMV- (ENSO+AMV-; Figs. 7e and 7f), negative SLP anomalies patterns are quite similar to those of ENSO+ in isolation (Fig. S6e); this suggests that AMV- has a limited amplifying effect on CWP extremes, in line with Fig. 6a.

A negative phase of ENSO (i.e., La Niña) is generally associated with the opposite phase of the PNA as compared to El Niño. Under the resulting combination PNA-ENSO- (Figs. 7g and 7h), which shows the largest positive effects on the population exposure (Fig. 6b), negative SLP anomalies are intensified over the North Asian region compared to those for modes in isolation (Figs. S6d and S6f). These intensified low-pressure conditions associated with storminess increase CWP extreme frequencies over a number of densely populated regions in North Asia and East Asia. PNA-ENSO- exemplifies how combined variability modes can lead to spatially compounding events by adding up the effects of individual modes in isolation. Specifically, under PNA-ENSO- the population exposed to extreme CWP extremes under PNA- and ENSO- in isolation partially adds up, resulting in spatially compounding events with a large population affected by CWP extremes.

https://doi.org/10.5194/egusphere-2024-2079
Preprint. Discussion started: 26 July 2024

Although the effects of combined variability modes ENSO-AMV+ (Figs. 7i and 7j) are rather limited, when combined with NAO+ (NAO+ENSO-AMV+; Figs. 7k and 7l) negative SLP anomalies are intensified over high latitudes, mainly due to NAO+ influence (Fig. S6a) and over South Asia, due to ENSO- (Fig. S6f). These intensified low-pressure systems lead to an amplification of CWP extremes in Northern Europe and South Asia. It is interesting to note that these two regions are not the same affected by ENSO-AMV+ (Figs. 7i-j), suggesting a strong influence of the NAO on regions impacted by CWP extremes.

Similar to what is observed for NAO-ENSO+, NAO-PNA+ENSO+ features a negative SLP anomaly extending across the Southern North Atlantic (Fig. 7n). However, for some regions, the addition of PNA+ to NAO-ENSO+ tends to weaken the effects of concurrent variability modes on CWP extremes, as some regions exhibit, on average, fewer regional CWP extremes than those obtained under NAO-ENSO+ (see blue boxes in Figs. 7n and 7m). A possible explanation may be that ENSO+ is weaker under PNA+ (Straus and Shukla, 2002), or model biases in the representation of extratropical stationary wave patterns (Park and Lee, 2021) and ENSO itself that can impact teleconnections to the North Pacific (Bayr et al., 2019).

4 Discussion

In this study, we present the first comprehensive assessment of the relation between individual and concurrent climate variability modes and the frequency of wintertime CWP extremes and associated spatially compounding events across regions of the Northern Hemisphere. We show that simulated concurrent modes are associated with an amplification of CWP extreme frequencies in many individual regions compared to variability modes in isolation. Simulations show that extreme spatially compounding events with many regions under CWP extremes in the same winter are enabled by positive dependencies between CWP extremes across different regions. Notably, such extreme spatially compounding events would not be possible without concurrent anomalies in variability modes. By changing the atmospheric circulation, concurrent variability modes amplify spatially compounding events, including the population affected by CWP extremes in the same winter, with ENSO being the most influential variability mode. We find that some of the concurrent modes, such as NAO-ENSO+ or ENSO+AMV-, that have a significant positive effect on spatially compounding events (Fig. 6) are also those that have effects on many individual regions (Figs. 3 and 4). This indicates that it is possible to make hypotheses about drivers of spatially compounding events by combining knowledge of common drivers of events across multiple individual regions.

A robust assessment of the effects of combined variability modes would not be possible using solely observations or reanalysis, due to the relatively short observational period (Singh et al., 2021; Bevacqua et al., 2023), therefore our results are primarily based on the CESM Single Model Initial-conditions Large Ensemble (SMILE) (Deser et al., 2020). Our model evaluation against ERA5 reanalysis data indicates that the simulated anomalies in CWP extremes associated with modes of variability are well suited for the purpose of our analysis (Figs. S2-S5) and thus we exploited the large sample size of a SMILE for a robust model-based analysis of compound events. Still, models have limitations (e.g., Cannon, 2018; Vrac, 2018; François et al., 2020), for example, related to possible biases for the magnitude of positive and negative phases of variability modes (e.g., Bellenger et al., 2014). Follow-up studies could consider large-ensemble simulations from more than one SMILE ensemble to test the sensitivity of the results with respect to the use of different models (Suarez-Gutierrez et al., 2021).

https://doi.org/10.5194/egusphere-2024-2079
Preprint. Discussion started: 26 July 2024

We analysed event counts aggregated over winter and at the scale of predefined SREX regions, given that high counts of compound extremes at these scales are expected to have negative effects on society. Still, the selected SREX regions may not reflect the natural spatial patterns of variation of CWP extremes. We also note that variability modes such as AMV or ENSO can have lagged effects on regional climate extremes (Ruiz-Barradas et al., 2000; Wang, 2019; Xing et al., 2022), an aspect that has been partially taken into account in this study for ENSO. Furthermore, additional variability modes than those considered here (e.g., the Indian Ocean Dipole (IOD), Qiu et al., 2014; Kurniadi et al., 2021) may be related to CWP frequencies in some regions, especially in the regions where the different combinations of the variability modes NAO, ENSO, PNA and AMV had no significant effects (in Fig. 3). In addition, the IOD is known to co-vary with some of the modes examined here, e.g. with ENSO and the AMV (Stuecker et al., 2017; Xue et al., 2022). Overall, although our aggregation in time and space may not be optimal for providing a fine-grained analysis of CWP events and additional modes may be relevant in some regions, our results align with known effects of modes of variability and expand current knowledge by providing information on rare compounding events. Among the identified hotspot regions where concurrent variability modes amplify CWP extremes, some are located in arid regions (e.g. Northern Africa), where CWP events may be less intense than in other regions. Still, detecting the effects of climate modes on arid regions is relevant for adaptation and mitigation policy because while CWP extremes can be a relevant source of freshwater (Berdugo et al., 2020), they can also pose a substantial flood hazard (e.g., Yin et al., 2023).

We mainly focused on the increase in the frequency of CWP extremes, however we note that increases in intensity at the same frequency, as well as low frequencies of CWP extremes may also be relevant information for the insurance industry (e.g., Ciullo et al., 2023). Studying the influence of variability modes on the intensity of the drivers (here, wind and precipitation) could further support mitigation and adaptation strategies (e.g., Whan and Zwiers, 2017; Li et al., 2022). Quantifying these effects on wind and precipitation in isolation would allow for a decomposition of the effects of concurrent variability modes, giving an even more complete picture of the processes involved (e.g., Manning et al., 2018; Brunner et al., 2021; Calafat et al., 2022). In addition, regarding spatial metrics, considering other relevant measures that combine return period information with the exposed population would allow for focusing on concurrent variability modes that regularly expose the population to CWP extremes.

With the methodology used here, it is not possible to thoroughly examine the causality behind the dependence between different variability modes and between the modes and CWP extremes. It is however clear that there exist important interactions and causal links between oceanic and atmospheric variability modes at different time scales, e.g., between ENSO and the NAO (Deser et al., 2017; Yeh et al., 2018), between the AMV and the NAO (Hurrell and Deser, 2010; Fang et al., 2018) and between ENSO and the PNA (Renwick and Wallace, 1996). Therefore, these modes are dependent on each other, a relevant information to take into account when investigating the causal effects of climate variability modes on characteristics of spatially compounding events. Applying advanced approaches such as causal networks (e.g., Nowack et al., 2020) may help to shed light on the complete causal pathway leading to spatially compounding events. We also note that dependencies among modes influence the return periods of concurrent modes, that is, certain signs of modes will co-occur with others more frequently than others, such as e.g. ENSO+NAO-, with an effect on their associated CWP extreme frequencies. In line with heterogeneous dependencies among different modes, we found a wide range of return periods for the different mode combinations (Fig. 3).

https://doi.org/10.5194/egusphere-2024-2079
Preprint. Discussion started: 26 July 2024

A natural continuation of this work is the application of the methodology developed in this study to investigate changes in CWP extremes over time, as well as their spatial relationships and dependencies with climate variability modes under climate change (Bevacqua et al., 2023).

5 Conclusions

We have identified groups of regions with positive spatial correlations between regional wintertime CWP extremes. These correlations enable extreme spatially compounding events with many regions experiencing CWP extremes during the same winter. We found that such extreme spatially compounding events, which also include a large fraction of the population of the Northern Hemisphere under CWP extremes in the same winter, are possible due to the combinations of multiple variability modes in anomalous phases. For example, combinations of modes nearly double the number of affected regions compared to neutral conditions on average. Among the modes, ENSO is found to be the most influential variability responsible for spatially compounding extreme events, which aligns with its known effects on weather and climate extremes worldwide (Goddard and Gershunov, 2020). The high return periods associated with some of the concurrent modes that lead to extreme spatially compounding events make it potentially difficult to factor these findings into long-term planning, e.g., infrastructure development or (re)insurance modelling. However, by identifying the drivers of the most extreme events, the findings raise awareness on the potential for extreme compounding events under certain mode combinations, which could be factored into weekly, subseasonal (White et al., 2022), seasonal (Lenssen et al., 2020) and longer forecasts to better anticipate mitigation action and climate services (Osman et al., 2023).

By using two different metrics to characterise spatially compounding events, we highlight that the effects of concurrent variability modes can differ from one spatial metric to another. While combinations with ENSO+ lead to the largest number of affected regions, when weighted by population exposure, combinations with ENSO- lead to higher effects on population. Our analysis thus stresses the importance of considering not only the interplay between variability modes but also a careful choice of metrics, which should be tailored to the ultimate impacts of interest, so as to assess the relevant characteristics of spatially compounding events and improve their risk management and mitigation.

Data availability. The ERA5 reanalysis data can be accessed via the "Climate Data Store" (CDS) web portal https://cds.climate.copernicus.eu/cdsapp#!/dataset/reanalysis-era5-single-levels. The CESM Large Ensemble Simulations can be downloaded from the CESM Large Ensemble Community Project website: https://www.earthsystemgrid.org/dataset/ucar.cgd.ccsm4.CLIVAR_LE.html. Modes of variability for CESM can be accessed via the CVDP-LE Data Repository https://www.cesm.ucar.edu/projects/cvdp-le/data-repository.

Author contributions. EB designed the initial plan of the study with DD. EB, LSG and DD supervised the project. EB, LSG, BF and KT designed the experiments and the statistical analyses with inputs from all co-authors. EB, KT and LSG provided the code for data pre-

https://doi.org/10.5194/egusphere-2024-2079
Preprint. Discussion started: 26 July 2024

processing. BF and KT made all computations and figures. BF, LB, RL, KT and LGS made the analyses and interpretations with inputs, corrections and additional writing contributions from EB, LSG and DD. BF wrote the first draft of the article with inputs from all co-authors.

Competing interests. The authors declare that they have no conflict of interest.

Acknowledgements. EB received funding from the Deutsche Forschungsgemeinschaft (DFG, German Research Foundation) via the Emmy Noether Programme (grant ID 524780515). LSG received funding from the European Union's Horizon Europe Framework Programme under the Marie Sklodowska-Curie grant agreement No 101064940. This project has received funding from the European Union's Horizon 2020 research and innovation programme under grant agreement No 101003469. This work emerged from the Training School on Dynamical Modelling of Compound Events organized by the European COST Action DAMOCLES (CA17109). This project has received funding from the European Research Council (ERC) under the European Union's Horizon 2020 research and innovation programme (Grant agreement No. 847456). Support from the Swiss National Science Foundation through project PP00P2_198896 to DD is gratefully acknowledged. We thank the NCAR's Climate Analysis Section for producing and making available the Climate Variability Diagnostics Package and the CESM simulations.

https://doi.org/10.5194/egusphere-2024-2079
Preprint. Discussion started: 26 July 2024

References

Bayr, T., Domeisen, D. I., and Wengel, C.: The effect of the equatorial Pacific cold SST bias on simulated ENSO teleconnections to the North Pacific and California, Climate Dynamics, 53, 3771–3789, 2019.

Bellenger, H., Guilyardi, E., Leloup, J., Lengaigne, M., and Vialard, J.: ENSO representation in climate models: from CMIP3 to CMIP5, Clim. Dyn., 42, 1999–2018, https://doi.org/10.1007/s00382-013-1783-z, 2014.

Berdugo, M., Delgado-Baquerizo, M., Soliveres, S., Hernández-Clemente, R., Zhao, Y., Gaitán, J. J., Gross, N., Saiz, H., Maire, V., Lehmann, A., Rillig, M. C., Solé, R. V., and Maestre, F. T.: Global ecosystem thresholds driven by aridity, Science, 367, 787–790, 2020.

Bevacqua, E., De Michele, C., Manning, C., Couasnon, A., Ribeiro, A. F. S., Ramos, A. M., Vignotto, E., Bastos, A., Blesić, S., Durante, F., Hillier, J., Oliveira, S. C., Pinto, J. G., Ragno, E., Rivoire, P., Saunders, K., van der Wiel, K., Wu, W., Zhang, T., and Zscheischler, J.: Guidelines for Studying Diverse Types of Compound Weather and Climate Events, Earth's Future, 9, e2021EF002 340, https://doi.org/10.1029/2021EF002340, e2021EF002340 2021EF002340, 2021a.

Bevacqua, E., Shepherd, T. G., Watson, P. A. G., Sparrow, S., Wallom, D., and Mitchell, D.: Larger Spatial Footprint of Wintertime Total Precipitation Extremes in a Warmer Climate, Geophysical Research Letters, 48, e2020GL091 990, https://doi.org/10.1029/2020GL091990, e2020GL091990 2020GL091990, 2021b.

Bevacqua, E., Suarez-Gutierrez, L., Jézéquel, A., Lehner, F., Vrac, M., Yiou, P., and Zscheischler, J.: Advancing research on compound weather and climate events via large ensemble model simulations, Nature Communications, 14, 2145, https://doi.org/10.1038/s41467-023-37847-5, 2023.

Bonferroni, C.: Teoria Statistica Delle Classi e Calcolo Delle Probabilita, Pubblicazioni del R Istituto Superiore di Scienze Economiche e Commerciali di Firenze (Libreria Internazionale Seeber, Florence, Italy), 8, 3–62, 1936.

Brunner, M. I., Swain, D. L., Gilleland, E., and Wood, A. W.: Increasing importance of temperature as a contributor to the spatial extent of streamflow drought, Environ. Res. Lett., 16, 024 038, https://doi.org/10.1088/1748-9326/abd2f0, 2021.

Calafat, F. M., Wahl, T., Tadesse, M. G., and Sparrow, S. N.: Trends in Europe storm surge extremes match the rate of sea-level rise, Nature, 603, 841–845, https://doi.org/10.1038/s41586-022-04426-5, 2022.

Cannon, A. J.: Multivariate quantile mapping bias correction: an N-dimensional probability density function transform for climate model simulations of multiple variables, Clim. Dynam., 50, 31–49, https://doi.org/10.1007/s00382-017-3580-6, 2018.

Ciullo, A., Strobl, E., Meiler, S., Martius, O., and Bresch, D. N.: Increasing countries' financial resilience through global catastrophe risk pooling, Nature Communications, 14, 922, https://doi.org/10.1038/s41467-023-36539-4, 2023.

Columbia University, C. f. I. E. S. I. N. . C.: Gridded Population of the World, Version 4 (GPWv4): Population Density, https://doi.org/10.7927/H4NP22DQ, 2016.

Davini, P., Hardenberg, J., and Corti, S.: Tropical origin for the impacts of the Atlantic Multidecadal Variability on the Euro-Atlantic climate, Environmental Research Letters, 10, 094 010, https://doi.org/10.1088/1748-9326/10/9/094010, 2015.

DelSole, T., Trenary, L., Tippett, M. K., and Pegion, K.: Predictability of Week-3–4 Average Temperature and Precipitation over the Contiguous United States, Journal of Climate, 30, 3499 – 3512, https://doi.org/10.1175/JCLI-D-16-0567.1, 2017.

Deser, C., Simpson, I. R., McKinnon, K. A., and Phillips, A. S.: The Northern Hemisphere Extratropical Atmospheric Circulation Response to ENSO: How Well Do We Know It and How Do We Evaluate Models Accordingly?, Journal of Climate, 30, 5059 – 5082, https://doi.org/10.1175/JCLI-D-16-0844.1, 2017.

https://doi.org/10.5194/egusphere-2024-2079
Preprint. Discussion started: 26 July 2024

Deser, C., Lehner, F., Rodgers, K. B., Ault, T., Delworth, T. L., DiNezio, P. N., Fiore, A., Frankignoul, C., Fyfe, J. C., Horton, D. E., Kay, J. E., Knutti, R., Lovenduski, N. S., Marotzke, J., McKinnon, K. A., Minobe, S., Randerson, J., Screen, J. A., Simpson, I. R., and Ting, M.: Insights from Earth system model initial-condition large ensembles and future prospects, Nature Climate Change, 10, 277–286, https://doi.org/10.1038/s41558-020-0731-2, 2020.

Domeisen, D. I., Butler, A. H., Fröhlich, K., Bittner, M., Müller, W. A., and Baehr, J.: Seasonal predictability over Europe arising from El Niño and stratospheric variability in the MPI-ESM seasonal prediction system, Journal of Climate, 28, 256–271, 2015.

Domeisen, D. I., Garfinkel, C. I., and Butler, A. H.: The teleconnection of El Niño Southern Oscillation to the stratosphere, Reviews of Geophysics, 57, 5–47, 2019.

Dowdy, A. and Catto, J.: Extreme weather caused by concurrent cyclone, front and thunderstorm occurrences, Scientific Reports, 7, 40 359, https://doi.org/10.1038/srep40359, 2017.

Fang, K., Chen, D., Ilvonen, L., Frank, D., Pasanen, L., Holmström, L., Zhao, Y., Zhang, P., and Seppä, H.: Time-varying relationships among oceanic and atmospheric modes: A turning point at around 1940, Quaternary International, 487, 12–25, https://doi.org/10.1016/j.quaint.2017.09.005, asia Pacific 2K, 2018.

Fischer, E. M., Beyerle, U., Bloin-Wibe, L., Gessner, C., Humphrey, V., Lehner, F., Pendergrass, A. G., Sippel, S., Zeder, J., and Knutti, R.: Storylines for unprecedented heatwaves based on ensemble boosting, Nature Communications, 14, 4643, https://doi.org/10.1038/s41467-023-40112-4, 2023.

Foulds, S. and Warburton, J.: Significance of wind-driven rain (wind-splash) in the erosion of blanket peat, Geomorphology, 83, 183–192, https://doi.org/10.1016/j.geomorph.2006.07.001, 2007.

François, B., Vrac, M., Cannon, A. J., Robin, Y., and Allard, D.: Multivariate bias corrections of climate simulations: Which benefits for which losses?, Earth Syst. Dyn., 11, 537–562, https://doi.org/10.5194/esd-2020-10, 2020.

Gampe, D., Schwingshackl, C., Böhnisch, A., Mittermeier, M., Sandstad, M., and Wood, R. R.: Applying global warming levels of emergence to highlight the increasing population exposure to temperature and precipitation extremes, Earth System Dynamics, 15, 589–605, https://doi.org/10.5194/esd-15-589-2024, 2024.

Garfinkel, C. and Hartmann, D.: Different ENSO teleconnections and their effects on the stratospheric polar vortex, Journal of Geophysical Research: Atmospheres, 113, 2008.

Goddard, L. and Gershunov, A.: Impact of El Niño on weather and climate extremes, El Niño Southern Oscillation in a changing climate, pp. 361–375, 2020.

Good, P.: Permutation Tests: A Practical Guide to Resampling Methods for Testing Hypotheses, Springer Science & Business Media, 2013.

Greeves, C., Pope, V., Stratton, R., and Martin, G.: Representation of Northern Hemisphere winter storm tracks in climate models, Clim. Dynam., 28, 683–702, https://doi.org/10.1007/s00382-006-0205-x, 2007.

Hansen, F., Kruschke, T., Greatbatch, R. J., and Weisheimer, A.: Factors Influencing the Seasonal Predictability of Northern Hemisphere Severe Winter Storms, Geophysical Research Letters, 46, 365–373, https://doi.org/10.1029/2018GL079415, 2019.

Hersbach, H., Bell, B., Berrisford, P., Hirahara, S., Horányi, A., Muñoz-Sabater, J., Nicolas, J., Peubey, C., Radu, R., Schepers, D., Simmons, A., Soci, C., Abdalla, S., Abellan, X., Balsamo, G., Bechtold, P., Biavati, G., Bidlot, J., Bonavita, M., De Chiara, G., Dahlgren, P., Dee, D., Diamantakis, M., Dragani, R., Flemming, J., Forbes, R., Fuentes, M., Geer, A., Haimberger, L., Healy, S., Hogan, R. J., Hólm, E., Janisková, M., Keeley, S., Laloyaux, P., Lopez, P., Lupu, C., Radnoti, G., de Rosnay, P., Rozum, I., Vamborg, F., Villaume, S., and Thépaut, J.-N.: The ERA5 global reanalysis, Q. J. R. Meteorol. Soc., 146, 1999–2049, https://doi.org/10.1002/qj.3803, 2020.

https://doi.org/10.5194/egusphere-2024-2079
Preprint. Discussion started: 26 July 2024

Hillier, J., Matthews, T., Wilby, R., and Murphy, C.: Multi-hazard dependencies can increase or decrease risk, Nat. Clim. Chang., 10, 1–4, https://doi.org/10.1038/s41558-020-0832-y, 2020.

Hong Lee, J., Julien, P. Y., and Lee, S.: Teleconnection of ENSO extreme events and precipitation variability over the United States, Journal of Hydrology, 619, 129 206, https://doi.org/10.1016/j.jhydrol.2023.129206, 2023.

Hu, S., Zhang, W., Jin, F.-F., Hong, L.-C., Jiang, F., and Stuecker, M. F.: Seasonal dependence of the Pacific–North American teleconnection associated with ENSO and its interaction with the annual cycle, Journal of Climate, 36, 7061–7072, 2023.

Hurrell, J. W. and Deser, C.: North Atlantic climate variability: The role of the North Atlantic Oscillation, Journal of Marine Systems, 79, 231–244, https://doi.org/10.1016/j.jmarsys.2009.11.002, impact of climate variability on marine ecosystems: A comparative approach, 2010.

Hurrell, J. W., Kushnir, Y., Ottersen, G., and Visbeck, M.: An Overview of the North Atlantic Oscillation, pp. 1–35, American Geophysical Union (AGU), ISBN 9781118669037, https://doi.org/10.1029/134GM01, 2003.

Iles, C. E., Vautard, R., Strachan, J., Joussaume, S., Eggen, B. R., and Hewitt, C. D.: The benefits of increasing resolution in global and regional climate simulations for European climate extremes, Geoscientific Model Development, 13, 5583–5607, https://doi.org/10.5194/gmd-13-5583-2020, 2020.

IPCC: *Climate Change 2021: The Physical Science Basis. Contribution of Working Group I to the Sixth Assessment Report of the Intergovernmental Panel on Climate Change* [Masson-Delmotte, V., P. Zhai, A. Pirani, S.L. Connors, C. Péan, S. Berger, N. Caud, Y. Chen, L. Goldfarb, M.I. Gomis, M. Huang, K. Leitzell, E. Lonnoy, J.B.R. Matthews, T.K. Maycock, T. Waterfield, O. Yelekçi, R. Yu, and B. Zhou (eds.)]., Cambridge University Press. In Press., 2021.

Iturbide, M., Gutiérrez, J. M., Alves, L. M., Bedia, J., Cerezo-Mota, R., Cimadevilla, E., Cofiño, A. S., Di Luca, A., Faria, S. H., Gorodetskaya, I. V., Hauser, M., Herrera, S., Hennessy, K., Hewitt, H. T., Jones, R. G., Krakovska, S., Manzanas, R., Martínez-Castro, D., Narisma, G. T., Nurhati, I. S., Pinto, I., Seneviratne, S. I., van den Hurk, B., and Vera, C. S.: An update of IPCC climate reference regions for subcontinental analysis of climate model data: definition and aggregated datasets, Earth System Science Data, 12, 2959–2970, https://doi.org/10.5194/essd-12-2959-2020, 2020.

Jeong, D. I., Cannon, A. J., and Morris, R. J.: Projected changes to wind loads coinciding with rainfall for building design in Canada based on an ensemble of Canadian regional climate model simulations, Climatic Change, 162, 821–835, https://doi.org/10.1007/s10584-020-02745-y, 2020.

Jiang, S., Tarasova, L., Yu, G., and Zscheischler, J.: Compounding effects in flood drivers challenge estimates of extreme river floods, Science Advances, 10, eadl4005, https://doi.org/10.1126/sciadv.adl4005, 2024.

Jiménez-Esteve, B. and Domeisen, D.: Nonlinearity in the North Pacific atmospheric response to a linear ENSO forcing, Geophysical Research Letters, 46, 2271–2281, 2019.

Jiménez-Esteve, B. and Domeisen, D. I.: Nonlinearity in the tropospheric pathway of ENSO to the North Atlantic, Weather and Climate Dynamics, 1, 225–245, 2020.

Jongman, B., Hochrainer-Stigler, S., Feyen, L., CJH, A., Mechler, R., Bouwer, L., Pflug, G., Rojas, R., and Ward, P.: Increasing Stress on Disaster-Risk Finance due to Large Floods, Nature Climate Change, 4, https://doi.org/10.1038/NCLIMATE2124, 2014.

Kay, J. E., Deser, C., Phillips, A., Mai, A., Hannay, C., Strand, G., Arblaster, J. M., Bates, S. C., Danabasoglu, G., Edwards, J., Holland, M., Kushner, P., Lamarque, J.-F., Lawrence, D., Lindsay, K., Middleton, A., Munoz, E., Neale, R., Oleson, K., Polvani, L., and Vertenstein, M.: The Community Earth System Model (CESM) Large Ensemble Project: A Community Resource for Studying Climate Change in the Pres-

https://doi.org/10.5194/egusphere-2024-2079
Preprint. Discussion started: 26 July 2024

ence of Internal Climate Variability, Bulletin of the American Meteorological Society, 96, 1333 – 1349, https://doi.org/10.1175/BAMS-D-13-00255.1, 2015.

Kelder, T., Wanders, N., van der Wiel, K., Marjoribanks, T. I., Slater, L. J., l Wilby, R., and Prudhomme, C.: Interpreting extreme climate impacts from large ensemble simulations—are they unseen or unrealistic?, Environmental Research Letters, 17, 044 052, https://doi.org/10.1088/1748-9326/ac5cf4, 2022.

Krichak, S. O. and Alpert, P.: Signatures of the NAO in the atmospheric circulation during wet winter months over the Mediterranean region, Theoretical and Applied Climatology, 82, 27–39, https://doi.org/10.1007/s00704-004-0119-7, 2005.

Kurniadi, A., Weller, E., Min, S.-K., and Seong, M.-G.: Independent ENSO and IOD impacts on rainfall extremes over Indonesia, International Journal of Climatology, 41, 3640–3656, https://doi.org/10.1002/joc.7040, 2021.

Lenssen, N. J., Goddard, L., and Mason, S.: Seasonal forecast skill of ENSO teleconnection maps, Weather and Forecasting, 35, 2387–2406, 2020.

Li, D., Chen, Y., Messmer, M., Zhu, Y., Feng, J., Yin, B., and Bevacqua, E.: Compound Wind and Precipitation Extremes Across the Indo-Pacific: Climatology, Variability, and Drivers, Geophysical Research Letters, 49, e2022GL098 594, https://doi.org/10.1029/2022GL098594, e2022GL098594 2022GL098594, 2022.

Li, W., Zhai, P., and Cai, J.: Research on the Relationship of ENSO and the Frequency of Extreme Precipitation Events in China, Advances in Climate Change Research, 2, 101–107, https://doi.org/10.3724/SP.J.1248.2011.00101, 2011.

Li, Z., Liu, J., Mauzerall, D. L., Li, X., Fan, S., Horowitz, L. W., He, C., Yi, K., and Tao, S.: A potential large and persistent black carbon forcing over Northern Pacific inferred from satellite observations, Scientific Reports, 7, 43 429, https://doi.org/10.1038/srep43429, 2017.

Liberato, M. L.: The 19 January 2013 windstorm over the North Atlantic: large-scale dynamics and impacts on Iberia, Weather. Clim. Extremes, 5-6, 16–28, https://doi.org/10.1016/j.wace.2014.06.002, 2014.

Lodise, J., Merrifield, S., Collins, C., Rogowski, P., Behrens, J., and Terrill, E.: Global Climatology of Extratropical Cyclones From a New Tracking Approach and Associated Wave Heights From Satellite Radar Altimeter, Journal of Geophysical Research: Oceans, 127, e2022JC018 925, https://doi.org/10.1029/2022JC018925, e2022JC018925 2022JC018925, 2022.

Maher, N., Milinski, S., and Ludwig, R.: Large ensemble climate model simulations: introduction, overview, and future prospects for utilising multiple types of large ensemble, Earth System Dynamics, 12, 401–418, https://doi.org/10.5194/esd-12-401-2021, 2021.

Manning, C., Widmann, M., Bevacqua, E., Loon, A. F. V., Maraun, D., and Vrac, M.: Soil Moisture Drought in Europe: A Compound Event of Precipitation and Potential Evapotranspiration on Multiple Time Scales, J. Hydrometeorol., 19, 1255–1271, https://doi.org/10.1175/JHM-D-18-0017.1, 2018.

Manning, C., Kendon, E. J., Fowler, H. J., Catto, J. L., Chan, S. C., and Sansom, P. G.: Compound wind and rainfall extremes: Drivers and future changes over the UK and Ireland, Weather and Climate Extremes, 44, 100 673, https://doi.org/10.1016/j.wace.2024.100673, 2024.

Martius, O., Pfahl, S., and Chevalier, C.: A global quantification of compound precipitation and wind extremes, Geophys. Res. Lett., 43, 7709–7717, https://doi.org/10.1002/2016GL070017, 2016.

Messmer, M. and Simmonds, I.: Global analysis of cyclone-induced compound precipitation and wind extreme events, Weather. Clim. Extremes, 32, 100 324, https://doi.org/10.1016/j.wace.2021.100324, 2021.

Mirrahimi, S., Lim, C. H., and Surat, S.: Review of method to estimation of wind-driven rain on building façade, Advances in Environmental Biology, 9, 18–23, 2015.

Müller, W. A. and Roeckner, E.: ENSO impact on midlatitude circulation patterns in future climate change projections, Geophysical Research Letters, 33, L05711, https://doi.org/10.1029/2005GL025032, 2006.

https://doi.org/10.5194/egusphere-2024-2079
Preprint. Discussion started: 26 July 2024

Niranjan Kumar, K. and Ouarda, T.: Precipitation variability over UAE and Global SST Teleconnections, Journal of Geophysical Research: Atmospheres, 119, https://doi.org/10.1002/2014JD021724, 2014.

Nowack, P., Runge, J., Eyring, V., and Haigh, J. D.: Causal networks for climate model evaluation and constrained projections, Nature Communications, 11, 1415, https://doi.org/10.1038/s41467-020-15195-y, 2020.

O'Reilly, C. H., Drouard, M., Ayarzagüena, B., Ambaum, M. H. P., and Methven, J.: The role of storm-track dynamics in the intraseasonal variability of the winter ENSO teleconnection to the North Atlantic, Quarterly Journal of the Royal Meteorological Society, 150, 2069–2086, https://doi.org/10.1002/qj.4691, 2024.

Osman, M., Domeisen, D., Robertson, A. W., and Weisheimer, A.: Sub-seasonal to decadal predictions in support of climate services, Climate Services, 30, 100 397, 2023.

Owen, L. E., Catto, J. L., Stephenson, D. B., and Dunstone, N. J.: Compound precipitation and wind extremes over Europe and their relationship to extratropical cyclones, Weather. Clim. Extremes, 33, 100 342, https://doi.org/10.1016/j.wace.2021.100342, 2021.

Park, M. and Lee, S.: Is the stationary wave bias in CMIP5 simulations driven by latent heating biases?, Geophysical Research Letters, 48, e2020GL091 678, 2021.

Phillips, A., Deser, C., and Fasullo, J.: Evaluating Modes of Variability in Climate Models, Eos, Transactions American Geophysical Union, 95, https://doi.org/10.1002/2014EO490002, 2014.

Pilorz, W., Laskowski, I., Surowiecki, A., and Łupikasza, E.: Fatalities related to sudden meteorological events across Central Europe from 2010 to 2020, International Journal of Disaster Risk Reduction, 88, 103 622, https://doi.org/10.1016/j.ijdrr.2023.103622, 2023.

Pinto, J. and Raible, C.: Past and recent changes in the North Atlantic oscillation, Wiley interdisciplinary reviews: Climate Change, 3, 79 – 90, https://doi.org/10.1002/wcc.150, 2012.

Pinto, J. G., Zacharias, S., Fink, A. H., Leckebusch, G. C., and Ulbrich, U.: Factors contributing to the development of extreme North Atlantic cyclones and their relationship with the NAO, Climate Dynamics, 32, 711–737, https://doi.org/10.1007/s00382-008-0396-4, 2009.

Qian, C., Ye, Y., Bevacqua, E., and Zscheischler, J.: Human influences on spatially compounding flooding and heatwave events in China and future increasing risks, Weather and Climate Extremes, 42, 100 616, https://doi.org/10.1016/j.wace.2023.100616, 2023.

Qiu, Y., Cai, W., Guo, X., and Ng, B.: The asymmetric influence of the positive and negative IOD events on China's rainfall, Scientific Reports, 4, 4943, https://doi.org/10.1038/srep04943, 2014.

Raveh-Rubin, S. and Catto, J. L.: Climatology and dynamics of the link between dry intrusions and cold fronts during winter, Part II: Front-centred perspective, Climate Dynamics, 53, 1893–1909, https://doi.org/10.1007/s00382-019-04793-2, 2019.

Raveh-Rubin, S. and Wernli, H.: Large-scale wind and precipitation extremes in the Mediterranean: a climatological analysis for 1979–2012, Q. J. Roy. Meteor. Soc., 141, 2404–2417, https://doi.org/10.1002/qj.2531, 2015.

Raymond, C., Suarez-Gutierrez, L., Kornhuber, K., Pascolini-Campbell, M., Sillmann, J., and Waliser, D. E.: Increasing spatiotemporal proximity of heat and precipitation extremes in a warming world quantified by a large model ensemble, Environ. Res. Lett., 17, 035 005, https://doi.org/10.1088/1748-9326/ac5712, 2022.

Renwick, J. A. and Wallace, J. M.: Relationships between North Pacific Wintertime Blocking, El Niño, and the PNA Pattern, Monthly Weather Review, 124, 2071 – 2076, https://doi.org/10.1175/1520-0493(1996)124<2071:RBNPWB>2.0.CO;2, 1996.

Ridder, N., Ukkola, A., Pitman, A., and Perkins-Kirkpatrick, S.: Increased occurrence of high impact compound events under climate change, NPJ Clim. Atmos. Sci., 5, https://doi.org/10.1038/s41612-021-00224-4, 2022.

Rivière, G. and Orlanski, I.: Characteristics of the Atlantic storm-track eddy activity and its relation with the North Atlantic Oscillation, Journal of the Atmospheric Sciences, 64, 241–266, 2007.

https://doi.org/10.5194/egusphere-2024-2079
Preprint. Discussion started: 26 July 2024

Rogers, J. C.: North Atlantic storm track variability and its association to the North Atlantic Oscillation and climate variability of northern Europe, Journal of Climate, 10, 1635–1647, 1997.

Ruiz-Barradas, A., Carton, J. A., and Nigam, S.: Structure of Interannual-to-Decadal Climate Variability in the Tropical Atlantic Sector, Journal of Climate, 13, 3285 – 3297, https://doi.org/10.1175/1520-0442(2000)013<3285:SOITDC>2.0.CO;2, 2000.

Sedgwick, P.: Multiple hypothesis testing and Bonferroni's correction, BMJ, 349, https://doi.org/10.1136/bmj.g6284, 2014.

Seneviratne, S., Nicholls, N., Easterling, D., Goodess, C., Kanae, S., Kossin, J., Luo, Y., Marengo, J., McInnes, K., Rahimi, M., Reichstein, M., Sorteberg, A., Vera, C., and Zhang, X.: Changes in climate extremes and their impacts on the natural physical environment. In: *Managing the Risks of Extreme Events and Disasters to Advance Climate Change Adaptation* [Field, C.B., V. Barros, T.F. Stocker, D. Qin, D.J. Dokken, K.L. Ebi, M.D. Mastrandrea, K.J. Mach, G.-K. Plattner, S.K. Allen, M. Tignor, and P.M. Midgley (eds.)], pp. 109–230, 2012.

Singh, J., Ashfaq, M., Skinner, C. B., Anderson, W. B., and Singh, D.: Amplified risk of spatially compounding droughts during co-occurrences of modes of natural ocean variability, npj Climate and Atmospheric Science, 4, 7, https://doi.org/10.1038/s41612-021-00161-2, 2021.

Straus, D. M. and Shukla, J.: Does ENSO force the PNA?, Journal of climate, 15, 2340–2358, 2002.

Stuecker, M. F., Timmermann, A., Jin, F.-F., Chikamoto, Y., Zhang, W., Wittenberg, A. T., Widiasih, E., and Zhao, S.: Revisiting ENSO/Indian Ocean dipole phase relationships, Geophysical Research Letters, 44, 2481–2492, 2017.

Suarez-Gutierrez, L., Milinski, S., and Maher, N.: Exploiting large ensembles for a better yet simpler climate model evaluation, Clim. Dynam., 57, 2557–2580, https://doi.org/10.1007/s00382-021-05821-w, 2021.

Taschetto, A., Ummenhofer, C., Stuecker, M., Dommenget, D., Ashok, K., Rodrigues, R., and Yeh, S.-W.: ENSO Atmospheric Teleconnections, pp. 309–335, ISBN 9781119548164, https://doi.org/10.1002/9781119548164.ch14, 2020.

Toniazzo, T. and Scaife, A. A.: The influence of ENSO on winter North Atlantic climate, Geophysical Research Letters, 33, https://doi.org/https://doi.org/10.1029/2006GL027881, 2006.

Trascasa-Castro, P., Ruprich-Robert, Y., Castruccio, F., and Maycock, A. C.: Warm Phase of AMV Damps ENSO Through Weakened Thermocline Feedback, Geophysical Research Letters, 48, e2021GL096 149, https://doi.org/10.1029/2021GL096149, e2021GL096149 2021GL096149, 2021.

Trenberth, K. E. and Shea, D. J.: Atlantic hurricanes and natural variability in 2005, Geophysical Research Letters, 33, https://doi.org/10.1029/2006GL026894, 2006.

van den Hurk, B. J., White, C. J., Ramos, A. M., Ward, P. J., Martius, O., Olbert, I., Roscoe, K., Goulart, H. M., and Zscheischler, J.: Consideration of compound drivers and impacts in the disaster risk reduction cycle, iScience, 26, 106 030, https://doi.org/10.1016/j.isci.2023.106030, 2023.

van der Wiel, K., Bloomfield, H. C., Lee, R. W., Stoop, L. P., Blackport, R., Screen, J. A., and Selten, F. M.: The influence of weather regimes on European renewable energy production and demand, Environmental Research Letters, 14, 094 010, https://doi.org/10.1088/1748-9326/ab38d3, 2019.

van Oldenborgh, G. J., Philip, S. Y., and Collins, M.: El Niño in a changing climate: a multi-model study, Ocean Science, 1, 81–95, https://doi.org/10.5194/os-1-81-2005, 2005.

Van Stan, J., Siegert, C., Levia, D., and Scheick, C.: Effects of wind-driven rainfall on stemflow generation between codominant tree species with differing crown characteristics, Agricultural and Forest Meteorology, 151, 1277, https://doi.org/10.1016/j.agrformet.2011.05.008, 2011.

https://doi.org/10.5194/egusphere-2024-2079
Preprint. Discussion started: 26 July 2024

Vrac, M.: Multivariate bias adjustment of high-dimensional climate simulations: the Rank Resampling for Distributions and Dependences (R^2D^2) bias correction, Hydrol. Earth Syst. Sci., 22, 3175–3196, https://doi.org/10.5194/hess-22-3175-2018, 2018.

Wahl, T., Jain, S., Bender, J., Meyers, S., and Luther, M.: Increasing risk of compound flooding from storm surge and rainfall for major US cities, Nat. Clim. Chang., 5, 1093–1097, https://doi.org/10.1038/nclimate2736, 2015.

Waliser, D. and Guan, B.: Extreme winds and precipitation during landfall of atmospheric rivers, Nature Geoscience, 10, 179–183, https://doi.org/10.1038/ngeo2894, 2017.

Wallace, J. M. and Gutzler, D. S.: Teleconnections in the Geopotential Height Field during the Northern Hemisphere Winter, Monthly Weather Review, 109, 784 – 812, https://doi.org/10.1175/1520-0493(1981)109<0784:TITGHF>2.0.CO;2, 1981a.

Wallace, J. M. and Gutzler, D. S.: Teleconnections in the geopotential height field during the Northern Hemisphere winter, Monthly weather review, 109, 784–812, 1981b.

Wang, C.: Three-ocean interactions and climate variability: a review and perspective, Climate Dynamics, 53, 5119–5136, https://doi.org/10.1007/s00382-019-04930-x, 2019.

Wang, C., Wang, B., Wu, L., and Luo, J.-J.: A Seesaw Variability in Tropical Cyclone Genesis between the Western North Pacific and the North Atlantic Shaped by Atlantic Multidecadal Variability, Journal of Climate, 35, 2479 – 2489, https://doi.org/10.1175/JCLI-D-21-0529.1, 2022.

Wang, J., Chen, Y., Tett, S. F. B., Stone, D., Nie, J., Feng, J., Yan, Z., Zhai, P., and Ge, Q.: Storyline attribution of human influence on a record-breaking spatially compounding flood-heat event, Science Advances, 9, eadi2714, https://doi.org/10.1126/sciadv.adi2714, 2023.

Whan, K. and Zwiers, F.: The impact of ENSO and the NAO on extreme winter precipitation in North America in observations and regional climate models, Climate Dynamics, 48, 1401–1411, https://doi.org/10.1007/s00382-016-3148-x, 2017.

White, C. J., Domeisen, D. I., Acharya, N., Adefisan, E. A., Anderson, M. L., Aura, S., Balogun, A. A., Bertram, D., Bluhm, S., Brayshaw, D. J., et al.: Advances in the application and utility of subseasonal-to-seasonal predictions, Bulletin of the American Meteorological Society, 103, E1448–E1472, 2022.

Xie, N., Sun, Y., and Gao, M.: The Influence of Five Teleconnection Patterns on Wintertime Extratropical Cyclones over Northwest Pacific, Atmosphere, 11, https://doi.org/10.3390/atmos11111248, 2020.

Xing, Z., Yu, Z., Wei, J., Zhang, X., Ma, M., Yi, P., Ju, Q., Wang, J., Laux, P., and Kunstmann, H.: Lagged influence of ENSO regimes on droughts over the Poyang Lake basin, China, Atmospheric Research, 275, 106 218, https://doi.org/10.1016/j.atmosres.2022.106218, 2022.

Xue, J., Luo, J.-J., Zhang, W., and Yamagata, T.: ENSO–IOD Inter-Basin Connection Is Controlled by the Atlantic Multidecadal Oscillation, Geophysical Research Letters, 49, e2022GL101 571, 2022.

Yeh, S.-W., Cai, W., Min, S.-K., McPhaden, M. J., Dommenget, D., Dewitte, B., Collins, M., Ashok, K., An, S.-I., Yim, B.-Y., and Kug, J.-S.: ENSO Atmospheric Teleconnections and Their Response to Greenhouse Gas Forcing, Reviews of Geophysics, 56, 185–206, https://doi.org/10.1002/2017RG000568, 2018.

Yin, J., Gao, Y., Chen, R., Yu, D., Wilby, R., Wright, N., Ge, Y., Bricker, J., Gong, H., and Guan, M.: Flash floods: why are more of them devastating the world's driest regions?, Nature, 615, 212–215, 2023.

Zhang, Y., Sun, X., and Chen, C.: Characteristics of concurrent precipitation and wind speed extremes in China, Weather and Climate Extremes, 32, 100 322, https://doi.org/10.1016/j.wace.2021.100322, 2021.

Zhao, H.: On the distinct interannual variability of tropical cyclone activity over the eastern North Pacific, Atmósfera, 28, 161–178, https://www.elsevier.es/en-revista-atmosfera-76-articulo-on-distinct-interannual-variability-tropical-S0187623617300024, 10.20937/ATM.2015.28.03.02, 2015.

https://doi.org/10.5194/egusphere-2024-2079
Preprint. Discussion started: 26 July 2024

Zscheischler, J., Westra, S., Hurk, B., Seneviratne, S., Ward, P., Pitman, A., AghaKouchak, A., Bresch, D., Leonard, M., Wahl, T., and Zhang, X.: Future climate risk from compound events, Nat. Clim. Chang., pp. 469–477, https://doi.org/10.1038/s41558-018-0156-3, 2018.

Zscheischler, J., Martius, O., Westra, S., Bevacqua, E., Raymond, C., Horton, R., Hurk, B., AghaKouchak, A., Jézéquel, A., Mahecha, M., Maraun, D., Ramos, A., Ridder, N., Thiery, W., and Vignotto, E.: A typology of compound weather and climate events, Nat. Rev. Earth Environ., 1, 1–5, 2020.

https://doi.org/10.5194/egusphere-2024-2079
Preprint. Discussion started: 26 July 2024

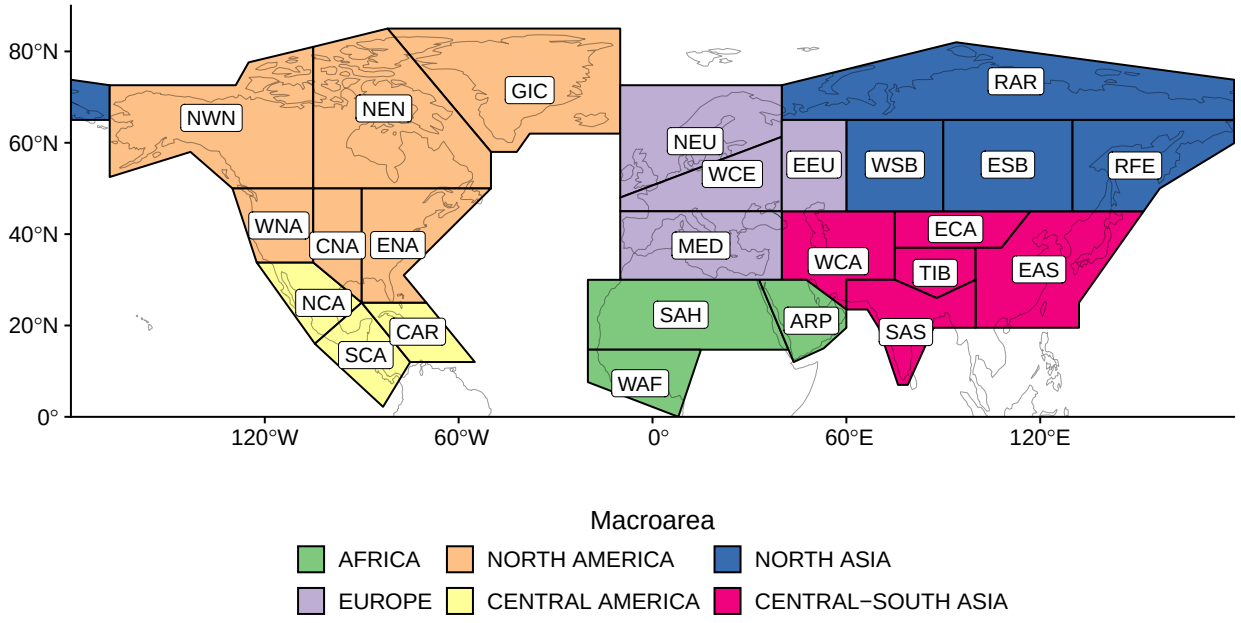

ARP	Arabian Peninsula	GIC	Greenland/Iceland	SAH	Sahara
CAR	Caribbean	MED	Mediterranean	SAS	South Asia
CNA	Central North America	NCA	North Central America	SCA	Southern Central America
EAS	East Asia	NEN	Northeastern North America	TIB	Tibetan Plateau
ECA	Eastern Central Asia	NEU	Northern Europe	WAF	Western Africa
EEU	Eastern Europe	NWN	Northwestern North America	WCA	Western Central Asia
ENA	East North America	RAR	Russian Arctic	WCE	West & Central Europe
ESB	Eastern Siberia	RFE	Russian Far East	WNA	Western North America
				WSB	Western Siberia

Figure 1. Presentation of the regions under study, that is the SREX regions (Iturbide et al., 2020) adopted by the Intergovernmental Panel on Climate Change (IPCC) in the Northern Hemisphere. The bottom part shows short and full names of the regions. Regions are clustered in macroareas (see legend). To balance the number of regions between continents, we partitioned the Asian continent into two macroareas (North Asia and Central-South Asia) and included the Arabic Peninsula (ARP) region in the Africa macroarea.

https://doi.org/10.5194/egusphere-2024-2079
Preprint. Discussion started: 26 July 2024

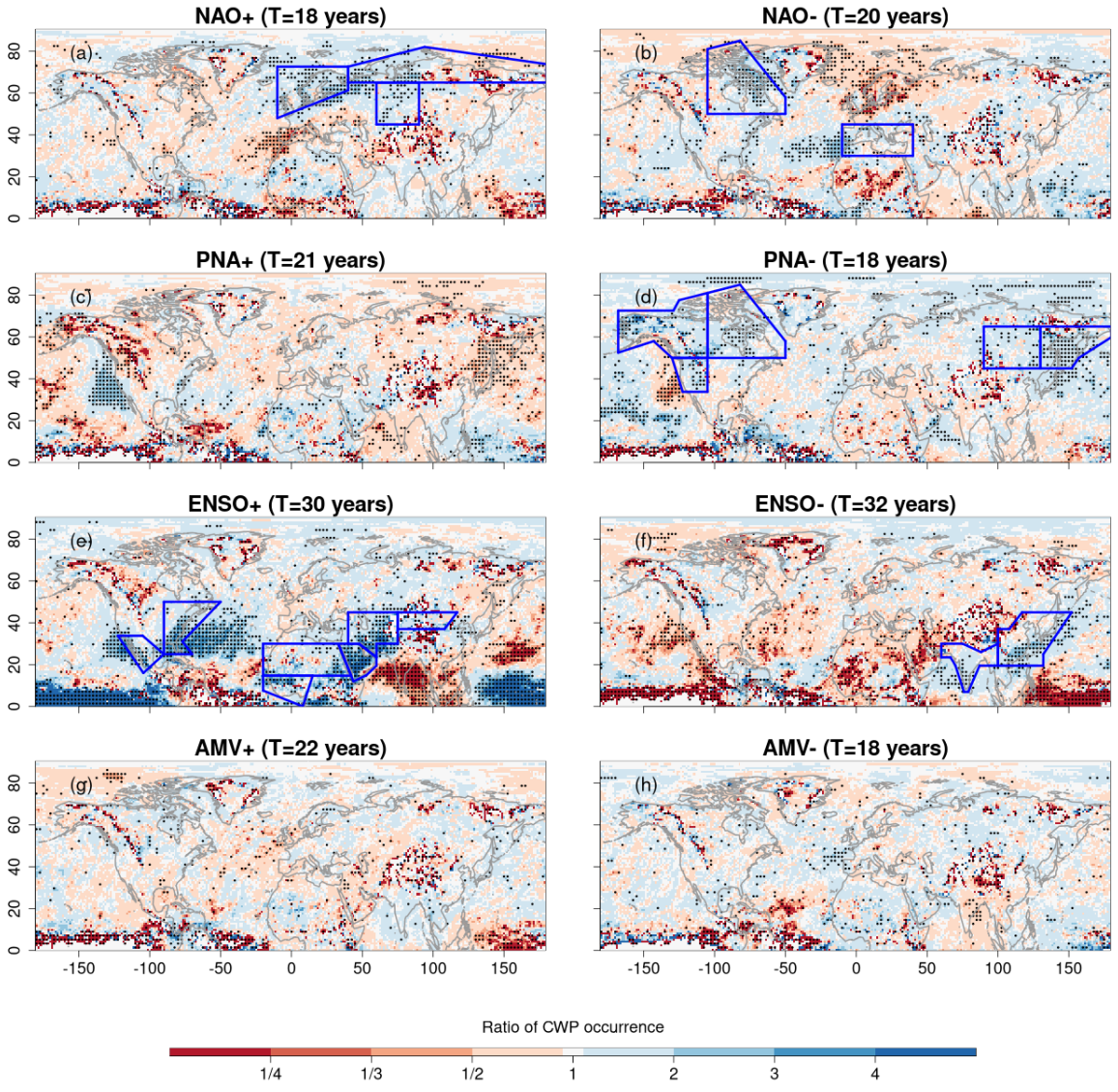

Figure 2. Direct effect of variability modes on wintertime compound wind and precipitation (CWP) extremes. Ratio of the average wintertime (December-February) CWP extreme frequencies for the (a) positive and (b) negative phases of NAO (while other variability modes are in their neutral phases) compared to neutral conditions (all variability modes being in their neutral phases) based on the CESM model. Corresponding maps are also displayed for (c, d) PNA, (e, f) ENSO and (g, h) AMV. Numbers in the headers indicate the empirical return period T (in years) for positive and negative phases of the variability modes (while other modes are in their neutral phases). The empirical return period for neutral conditions (i.e., when all modes are in their neutral phases) is T=3 years. Stippling indicates significant differences of mean frequency relative to neutral conditions at the 10% significance level using permutation tests (two-sided) with Bonferroni correction. The framed regions in blue are those where the direct effects of variability modes significantly increase regionally averaged CWP extreme frequencies compared with neutral conditions (following the methodology defined in subsection 2.2.3, and reflecting information in Fig. 3).

https://doi.org/10.5194/egusphere-2024-2079
Preprint. Discussion started: 26 July 2024

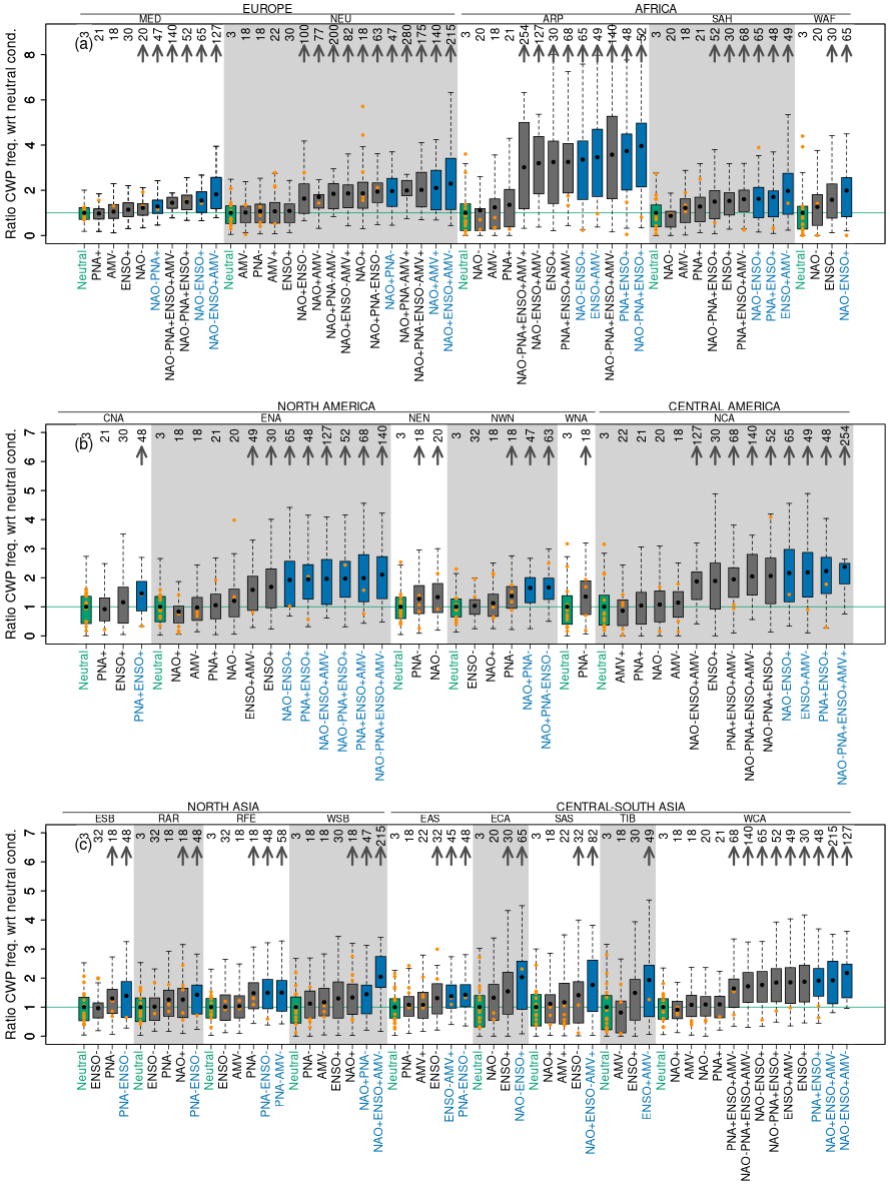

Figure 3. Influence of concurrent variability modes on regional compound wind and precipitation (CWP) extremes. Ratio of the regionally averaged wintertime CWP extreme frequencies for the relevant individual and concurrent variability modes (following the methodology defined in subsection 2.2.3) with respect to average frequency for neutral conditions based on the CESM model (orange dots represent associated values of the ratio derived from ERA5, when available, with each dot representing one winter season). Results are displayed for (a) Europe and Africa, (b) North America and Central America, and (c) Northern Asia and Central-South Asia. The empirical return periods (in years) for individual and concurrent variability modes are indicated on the top. Grey arrows indicate significant differences in the mean frequency relative to neutral conditions (at the 10% significance level, with Bonferroni correction). Green boxes indicate distributions for neutral conditions (all variability modes being in their neutral phases) and green horizontal lines indicate ratios equal to one. Blue boxes indicate mode combinations with amplified effects, that is higher means of regionally averaged CWP extreme frequencies than their underlying mode sub-combinations (methods subsection 2.2.3). We remove concurrent variability modes that occur in less than 10 winters and regions without significant effects arrows (EEU, WCE, GIC, CAR and SCA).

https://doi.org/10.5194/egusphere-2024-2079
Preprint. Discussion started: 26 July 2024

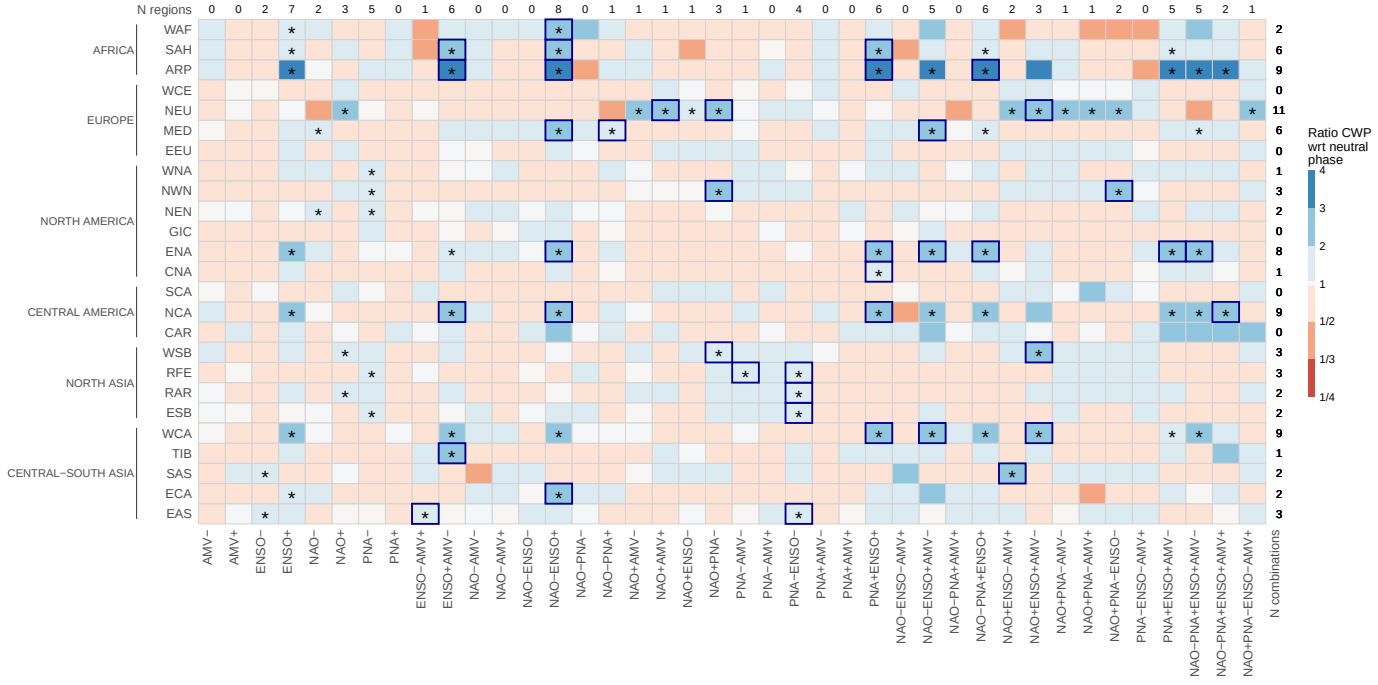

Figure 4. Effects of variability modes on wintertime compound wind and precipitation (CWP) extremes in SREX regions. For different regions (see labels on the left side of the matrix), the ratio of the regionally averaged CWP extreme frequencies for individual and concurrent variability modes (see labels on the bottom side of the matrix) with respect to the average frequency under neutral phases of all modes (Metric 1, see Methods), based on the CESM model. Note that positive effects of concurrent variability modes (ratio above 1) tend to be stronger than negative effects (ratio below 1). The individual and concurrent variability modes with significant effects (at the 10% level with Bonferroni correction) relative to neutral conditions are indicated with an asterisk. Blue cell borders indicate combinations with higher means of regionally averaged CWP extreme frequencies than their underlying mode sub-combinations (methods in subsection 2.2.3). To ensure robustness, we do not display concurrent variability modes that occur in less than 10 winters. Based on the displayed information, the numbers on the top and right margins indicate the total count of regions and mode combinations with significant effects of modes, respectively.

https://doi.org/10.5194/egusphere-2024-2079
Preprint. Discussion started: 26 July 2024

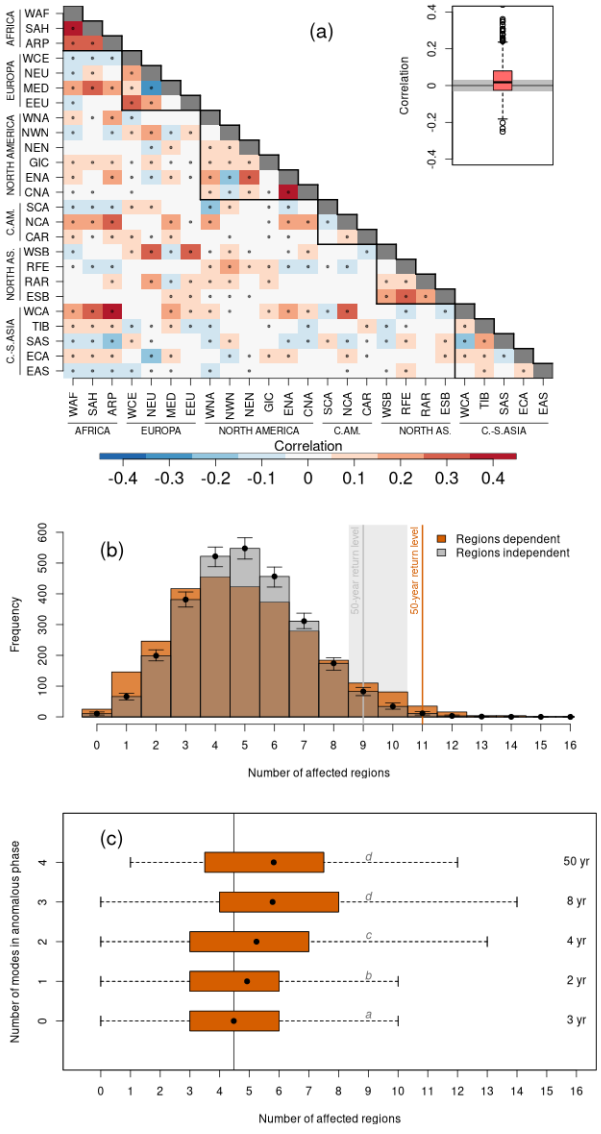

Figure 5. Dependencies between regional wintertime compound wind and precipitation (CWP) extremes. (a) Matrix of Spearman correlations for regionally averaged wintertime (December-February) CWP extreme frequencies between regions based on the CESM model. Stippling indicates significant correlations (correlation values that are outside the 90% centred confidence interval). A contour is added for regions in the same macroarea. The boxplot shows summaries of the distribution of the correlations shown in the matrix (interquartile range, median and outliers); the grey background shows the confidence interval for no correlation (bootstrap-based 90% range). (b) Histograms of the number of regions with a high frequency of CWP extremes during the same winter based on the CESM model (orange histogram) and when assuming independence between regional wintertime CWP extreme frequencies (grey histogram; obtained via shuffling the data 1000 times via bootstrap). Vertical lines show the 50-year return levels under dependence and independence. Bootstrap-based confidence intervals for each bin and 50-year return level at 10% significance level are also shown. (c) Boxplots of the number of affected regions given different numbers of variability modes in anomalous phases. The empirical return periods (in years) for the different number of variability modes in anomalous phases are indicated on the right. Mean of the ratios under a different number of modes in anomalous phases that are not significantly different ($\alpha = 0.10$, one-sided permutation test) are indicated with the same letters (Jiang et al., 2024). The average number of regions affected under neutral conditions is indicated by a vertical line.

https://doi.org/10.5194/egusphere-2024-2079
Preprint. Discussion started: 26 July 2024

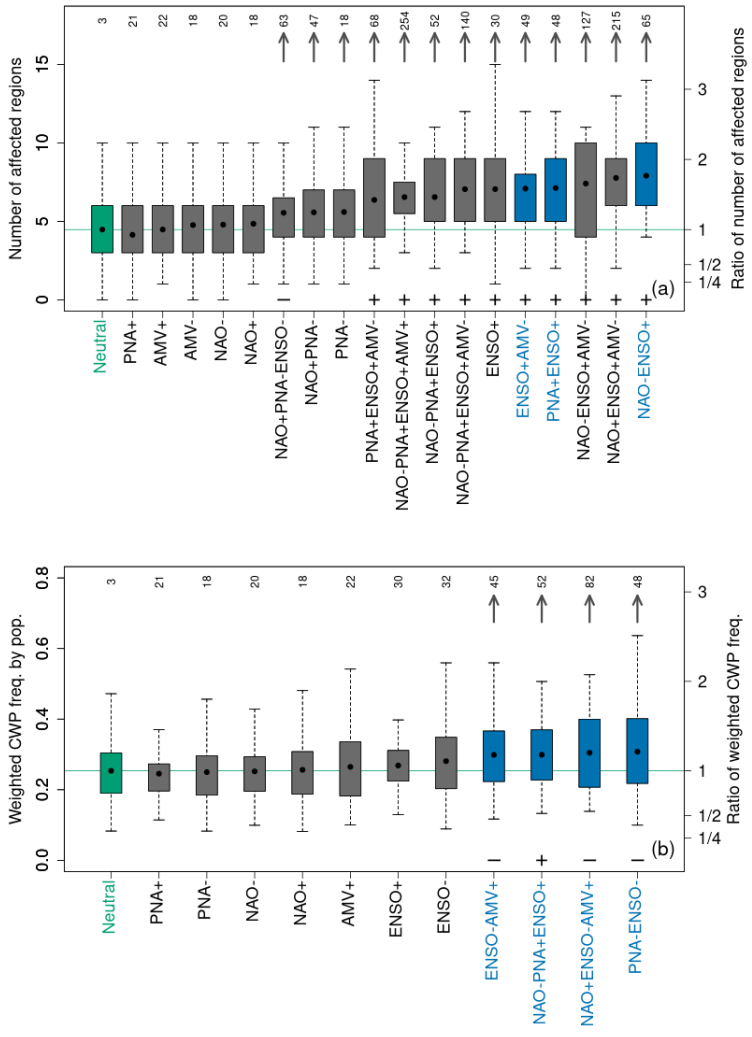

Figure 6. Influence of variability modes on spatially compounding wind and precipitation (CWP) extremes. (a) Distributions of the number of regions (left y-axis) experiencing a high frequency of CWP extremes during the same winter (December-February) for different individual and concurrent variability modes (x-axis), based on the CESM model. The right y-axis shows the ratio of the metric to its average under neutral phases of all modes. The combinations presented are selected according to the methodology defined in subsection 2.2.3. Grey arrows indicate significant differences in the mean with respect to neutral conditions at the 10% significance level using one-sided permutation tests and Bonferroni correction. Green boxes indicate distributions for neutral conditions (all variability modes being in their neutral phases). Blue boxes indicate combinations exhibiting higher means than their underlying mode sub-combinations (methods subsection 2.2.3). (b) The same as panel (a), but for the population-weighted CWP extremes over the Northern Hemisphere. Symbols + and − above the x-axis in panels (a) and (b) highlight combinations having a significant effect for a metric containing ENSO+ and ENSO-, respectively.

https://doi.org/10.5194/egusphere-2024-2079
Preprint. Discussion started: 26 July 2024

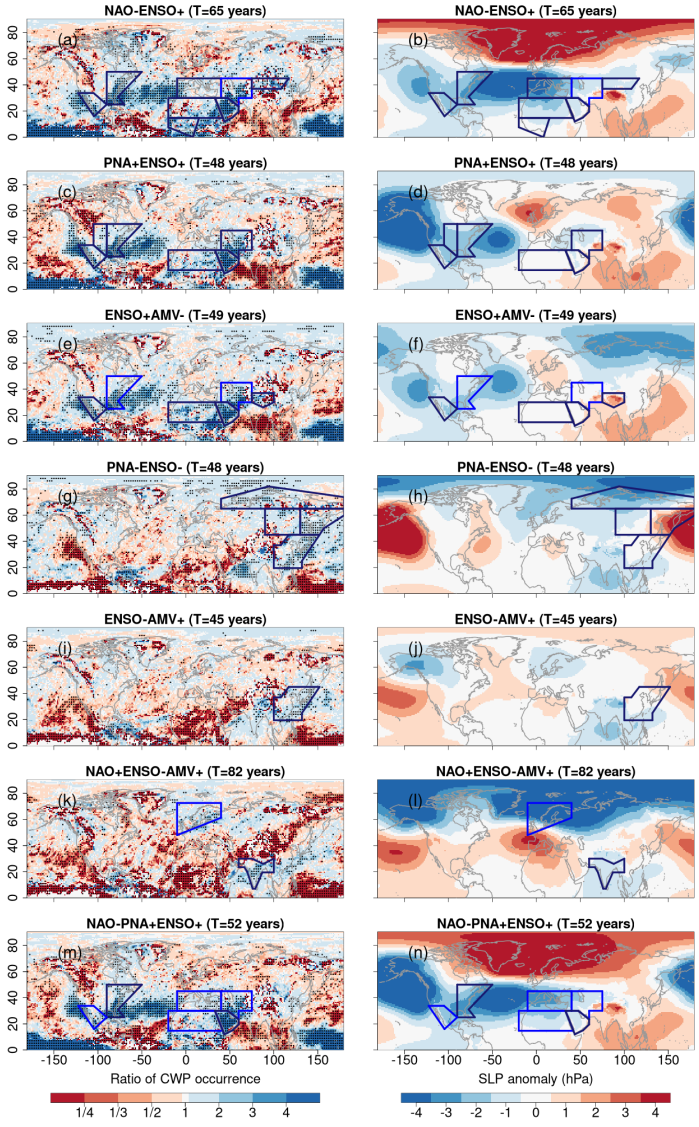

Figure 7. Compound wind and precipitation (CWP) extremes for concurrent anomalies in variability modes and associated sea level pressure anomalies. (a) Ratio of the average wintertime (December-February) CWP frequencies for the concurrent variability mode NAO-ENSO+ (while other variability modes are in their neutral phases) compared to winter with all variability modes in neutral phases, based on the CESM model. (b) Mean sea level pressure anomalies for NAO-ENSO+ (while other variability modes are in their neutral phases) compared to neutral conditions (all variability modes being in their neutral phases) based on the CESM model. Corresponding maps are also displayed for (c, d) PNA+ENSO+, (e, f) ENSO+AMV-, (g, h) PNA-ENSO-, (i, j) ENSO-AMV+, (k, l) NAO+ENSO-AMV+ and (m, n) NAO-PNA+ENSO+. Numbers in the headers indicate the empirical return period T (in years) for the different concurrent variability modes stated in the title of the panels, whereas the return period for neutral conditions (all modes are in their neutral phases) is T=3 years. Stippling indicates significant differences in mean frequency relative to neutral conditions at the 10% significance level using permutation tests (two-sided) with Bonferroni correction. The framed regions are those where concurrent variability modes significantly increase regionally averaged CWP extreme frequencies compared with neutral conditions; by reflecting information in Fig. 3, the dark framing indicates an amplified effect with respect to underlying mode sub-combinations (methods in subsection 2.2.3).